CHEMISTRY
A EUROPEAN JOURNAL

DOI: 10.1002/chem.200701108

Molecular and Electronic Structures of One-Electron Oxidized Ni^{II}–(Dithiosalicylidenediamine) Complexes: Ni^{III}–Thiolate versus Ni^{II}–Thiyl Radical States

Philip A. Stenson, Ashley Board, Armando Marin-Becerra, Alexander J. Blake, E. Stephen Davies, Claire Wilson, Jonathan McMaster,* and Martin Schröder*[a]

Abstract: The dithiosalicylidenediamine Ni^{II} complexes [Ni(L)] (R = *t*Bu, R′ = $CH_2C(CH_3)_2CH_2$ **1**, R′ = C_6H_4 **2**; R = H, R′ = $CH_2C(CH_3)_2CH_2$ **3**, R′ = C_6H_4 **4**) have been prepared by transmetallation of the tetrahedral complexes [Zn(L)] (R = *t*Bu, R′ = $CH_2C(CH_3)_2CH_2$ **7**, R′ = C_6H_4 **8**; R = H, R′ = $CH_2C(CH_3)_2CH_2$ **9**, R′ = C_6H_4 **10**) formed by condensation of 2,4-di-R-thiosalicylaldehyde with diamines H_2N-R′-NH_2 in the presence of Zn^{II} salts. The diamagnetic mononuclear complexes [Ni(L)] show a distorted square-planar N_2S_2 coordination environment and have been characterized by ^{1}H- and ^{13}C NMR and UV/Vis spectroscopies and by single-crystal X-ray crystallography. Cyclic voltammetry and coulombic measurements have established that complexes **1** and **2**, incorporating *t*Bu functionalities on the thiophenolate ligands, undergo reversible one-electron oxidation processes, whereas the analogous redox processes for complexes **3** and **4** are not reversible. The one-electron oxidized species, $\mathbf{1}^+$ and $\mathbf{2}^+$, can be generated quantitatively either electrochemically or chemically with 70% $HClO_4$. EPR and UV/Vis spectroscopic studies and supporting DFT calculations suggest that the SOMOs of $\mathbf{1}^+$ and $\mathbf{2}^+$ possess thiyl radical character, whereas those of $\mathbf{1}(py)_2^+$ and $\mathbf{2}(py)_2^+$ possess formal Ni^{III} centers. Species $\mathbf{2}^+$ dimerizes at low temperature, and an X-ray crystallographic determination of the dimer $[(\mathbf{2})_2](ClO_4)_2 \cdot 2CH_2Cl_2$ confirms that this dimerization involves the formation of a S–S bond (S···S = 2.202(5) Å).

Keywords: CO dehydrogenase · hydrogenases · nickel · redox chemistry · superoxide dismustase · thiolate

Introduction

There is considerable support for the participation of the Ni^{III} oxidation state in the catalytic cycles of the [NiFe] hydrogenases,[1,2] acetyl coenzyme A synthase (ACS),[3–5] CO dehydrogenase,[6,7] methyl coenzyme M reductase,[8] and Ni-containing superoxide dismustase (NiSOD).[9,10] A common feature of all of these enzymes is cysteine-thiolate coordination at the Ni center in the active site. The S-ligation has been proposed to lower the redox potential of the metal unit in these enzymes.[1c,10] NiSOD catalyses the disproportionation of the superoxide radical to hydrogen peroxide and dioxygen via a two-step, ping-pong mechanism involving a monomeric Ni center that cycles between the formal Ni^{II} and Ni^{III} oxidation states.[11,12] X-ray crystallographic studies on the oxidized[9] and reduced[10] forms of the enzyme from *Streptomyces* reveal that in the reduced Ni^{II} state the enzyme is coordinated in a square-planar N_2S_2 arrangement by two thiolate ligands derived from Cys2 and Cys6, the deprotonated amide of the Cys2 backbone, and the N-terminal -NH_2 group of His1. On oxidation, the Ni center adopts a square-pyramidal geometry containing the same equatorial ligand set as for the reduced form, but with an additional His1 imidazole ligand bound in the axial position (Figure 1).

Thus, during the catalytic cycle the metal undergoes a change in its coordination sphere with the binding of His1 in the oxidized form of the enzyme playing a critical role in the catalytic mechanism. Detailed spectroscopic and supporting theoretical calculations on the enzyme and related model complexes suggest that the imidazole group of His1

[a] Dr. P. A. Stenson, A. Board, Dr. A. Marin-Becerra, Prof. Dr. A. J. Blake, Dr. E. S. Davies, Dr. C. Wilson, Prof. Dr. J. McMaster, Prof. Dr. M. Schröder
School of Chemistry, University of Nottingham, Nottingham, NG7 2RD (UK)
Fax: (+44) 115-951-3563
E-mail: j.mcmaster@nottingham.ac.uk
m.schroder@nottingham.ac.uk

Supporting information for this article is available on the WWW under http://www.chemeurj.org/ or from the author.

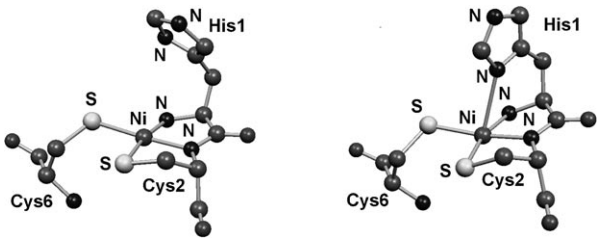

Figure 1. The structures of the active site of a) the reduced form of NiSOD[9] and b) the oxidized form of NiSOD.[10]

needs to coordinate to the metal center following oxidation to form a stable Ni^{III} species at the active site of the enzyme.[13,14] The axial coordination of the imidazole group from His1 forces the unpaired electron into a Ni d_{z^2}-based molecular orbital that possesses little thiolate character, thereby suppressing thiolate-based oxidative chemistry that could result in the formation of sulfonate groups which may inactivate the enzyme. Previous studies of $[Ni^{II}(N_2S_2)]^n$ ($n=$ 0, 2−) compounds have demonstrated this irreversible oxidation at the thiolate ligands. For example, the species $[Ni^{II}(N_2S_2)]^0$ containing neutral amine N-donors can react with dioxygen to form sulfonate ligands[15] and form disulfide species on one-electron electrochemical oxidation.[16] In contrast, complexes of the type $[Ni^{II}N_2S_2]^{2-}$ containing anionic amide N-donors exhibit reversible electrochemistry that ultimately leads to the generation of Ni^{III} centers that can be detected as their pyridine adducts by EPR spectroscopy in solution at low temperature.[17–19] There is one example of a synthetic complex containing a mixed amine/amide thiolate coordination sphere $[Me_4N][Ni^{II}(BEAAM)]$ (BEAAM = *N*-{2-[benzyl-(2-mercapto-2-methylpropyl)amino]ethyl}-2-mercapto-2-methylpropionamide), which has been shown to exhibit reversible metal-based redox chemistry but with spectroscopic properties that are intermediate between those of $[Ni(N_2S_2)]$ complexes containing exclusively N-amine or N-amide coordination.[20] It has been argued that the mixed amine/amide coordination at the active site of NiSOD plays a crucial role in tuning the redox chemistry and reactivity of the active site.[13,14] Thus, filled–filled interactions between the π-donating amide ligand and the Ni–π orbitals destabilize metal-based orbitals, thereby facilitating electron transfer from Ni^{II} to $O_2^{\bullet-}$ to generate a Ni^{III} center, rather than S-based radicals, in the catalytic cycle.

We report herein the chemistry of a series of Ni complexes of the type $[Ni(N_2S_2)]$ incorporating imine N-donors within the ligand framework to probe the effect of the incorporation of these N-donors on the electronic structure of a $[Ni(N_2S_2)]$ center. These N-donors are expected to possess different σ- and π-properties compared to amine and amide N-donors, features that appear to be important determinants of the nature of the SOMO within the oxidized species. We have been interested in the study of a range of unusual metal oxidation state and ligand–radical species based on S-donor ligation,[21] particularly with Ni and related centers,[22] and describe herein the synthesis and spectroscopic characterization of the redox-active mononuclear complexes [Ni(L)] **1**–**4**, where L is derived from the condensation of 2,4-di-R-thiosalicylaldehyde with 2-dimethyl-1,3-diaminopropane (R = *t*Bu, **1**; H, **3**) or 1,2-benzenediamine (R = *t*Bu, **2**; H, **4**, Scheme 1). Electrochemistry, EPR and UV/Vis spectroscopies, and supporting DFT calculations have been employed to probe the electronic structures of electrochemically and chemically generated $[Ni(L)]^+$ and $[Ni(L)(py)_2]^+$ to gain insight into the role of the coordination sphere in controlling the nature of the electronic structure of the active site of NiSOD.

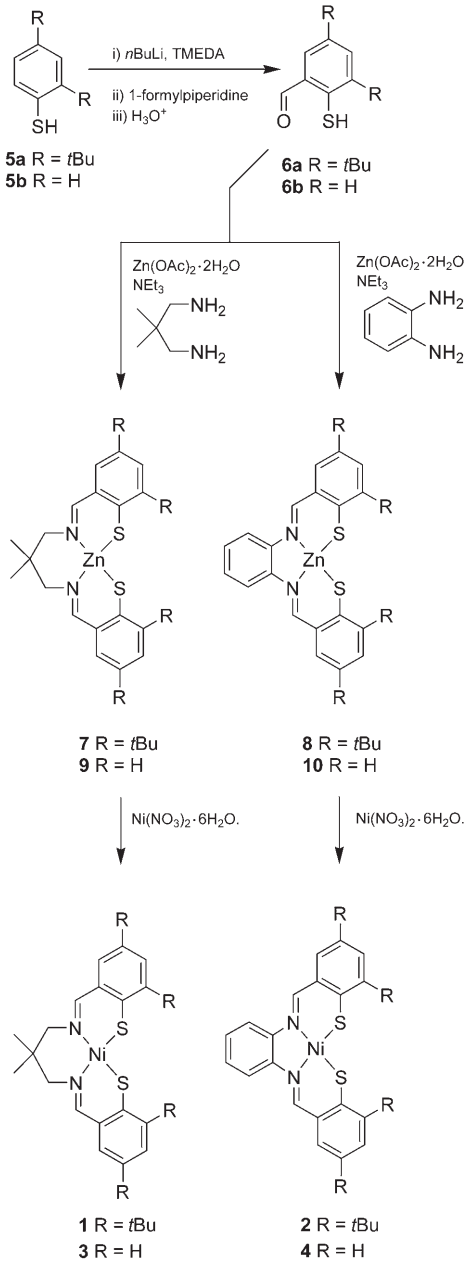

Scheme 1. Schematic representation of the synthesis of complexes **1**–**4**.

Results and Discussion

Synthesis of ligands and Zn^{II} complexes: 2,4-Di-*tert*-butylbenzenethiol (**5a**) was obtained by reaction of 2,4-di-*tert*-butylbromobenzene with Mg in Et_2O followed by quenching of the Grignard reagent with sulfur as we have reported previously for **5b**.[23] Ortho-formylation of **5a** to yield aldehyde **6a** was achieved following modified literature procedures.[24–26] The use of 1-formylpiperidine as formylating agent in place of the previously reported *N,N*-dimethylformamide increased the yield from about 55% to about 80%. ^{1}H NMR spectra of crude **6a** confirmed that the main contaminant was **5a**. However, a comprehensive purification procedure of **6a** was not sought as the crude product reacted cleanly with 2-dimethyl-1,3-diaminopropane or 1,2-benzenediamine and $Zn(OAc)_2$ via a template Schiff-base condensation reaction to afford **7**–**10**, which crystallized readily in yields of 80–90%.

Analytically pure yellow crystals of **7** and **9**, and red crystals of $(\mathbf{8})_2$ were obtained by recrystallization of the crude products. ^{1}H NMR and ^{13}C NMR spectra were consistent with the formation of diamagnetic Schiff-base Zn^{II} complexes, which was confirmed by single-crystal X-ray crystallographic studies of **7**, $(\mathbf{8})_2$, and **9**. Selected bond lengths and angles for these complexes are shown in Table 1. Complexes **7** and **9** (Figure 2) reveal monomeric Zn^{II} centers possessing a distorted tetrahedral N_2S_2 coordination sphere about the Zn^{II} center (the angle between the planes defined by S-Zn-S and N-Zn-N is 86.0° and 66.7°, for **7** and **9**, respectively). The solid-state structure of $(\mathbf{8})_2$ reveals a thiolate-bridged dimer with two $Zn(N_2S_2)$ units linked by two μ_2-S bridging interactions to form a Zn_2S_2 diamond core (Figure 3). The geometry at Zn^{II} may be described as distorted trigonal bipyramidal in which, for Zn(1), S(1) and N(2) occupy axial positions and, for Zn(2), S(2′) and N(1′) are the axial donor atoms. The $Zn(\mu\text{-}S)_2Zn$ core forms a butterfly motif in which the bridging thiolate S-donors form the apex of a hinge with Zn(1)···Zn(2) = 3.287(2) Å. The bond lengths around Zn^{II} are consistent with those reported previously for similar Zn^{II} complexes with N_2S_2 coordination.[27–32]

Synthesis of Ni^{II} complexes: The Ni^{II} complexes **1**–**4** were prepared from the corresponding Zn^{II} complexes **7**–**10**, respectively, via transmetallation with $Ni(NO_3)_2{\cdot}6H_2O$ in $MeOH/CH_2Cl_2$ solution (Scheme 1). The substitution of Zn^{II} by Ni^{II} is accompanied by a change in color of the solution from yellow to dark brown, and traces of $Zn(NO_3)_2$ in the crude product were removed by washing with MeOH. The overall yield using this procedure is improved greatly

Table 1. Selected bond lengths [Å] and angles [°] for **7**, $(\mathbf{8})_2$ and **9**.

	7[a]	$(\mathbf{8})_2$	**9**
Zn(1)−S(1)	2.2573(7)	2.3885(5)	2.2762(9)
Zn(1)−S(2)	2.2573(7)	2.3139(5)	2.2564(9)
Zn(1)−N(1)	2.018(2)	2.143(2)	2.044(2)
Zn(1)−N(2)	2.018(2)	2.080(2)	2.035(2)
N(1)−C(1)	1.278(3)	1.295(2)	1.265(4)
N(2)−C(1A)	1.278(3)	1.276(2)	1.281(4)
Zn(1)−S(2′)		2.4811(5)	
Zn(2)−S(1)		2.4493(5)	
Zn(2)−S(1′)		2.2838(5)	
Zn(2)−S(2′)		2.4284(5)	
Zn(2)−N(1′)		2.107(2)	
Zn(2)−N(2′)		2.152(2)	
N(1′)−C(1B)		1.280(2)	
N(2′)−C(1C)		1.297(2)	
S(1)-Zn(1)-S(2)	124.78(4)	108.04(2)	117.95(4)
S(1)-Zn(1)-N(1)	96.46(6)	89.21(4)	96.92(7)
S(1)-Zn(1)-N(2)	123.25(8)	162.75(5)	126.70(7)
S(2)-Zn(1)-N(1)	123.25(8)	126.82(4)	127.86(7)
S(2)-Zn(1)-N(2)	96.46(6)	89.12(5)	98.10(7)
N(1)-Zn(1)-N(2)	89.05(14)	78.70(6)	88.80(10)
S(1′)-Zn(2)-S(2′)		100.85(2)	
S(1′)-Zn(2)-N(1′)		91.97(4)	
S(1′)-Zn(2)-N(2′)		128.10(4)	
S(2′)-Zn(2)-N(1′)		163.52(4)	
S(2′)-Zn(2)-N(2′)		86.25(4)	
N(1′)-Zn(2)-N(2′)		77.66(6)	
S(1)-Zn(1)-S(2′)		79.62(2)	
S(1)-Zn(2)-S(2′)		79.49(2)	
Zn(1)-S(1)-Zn(2)		85.60(2)	
Zn(1)-S(2′)-Zn(2)		84.06(2)	

[a] Half of the complex is crystallographically independent with the geometry completed by a twofold rotation, $1-x, y, -z + {}^1/_2$.

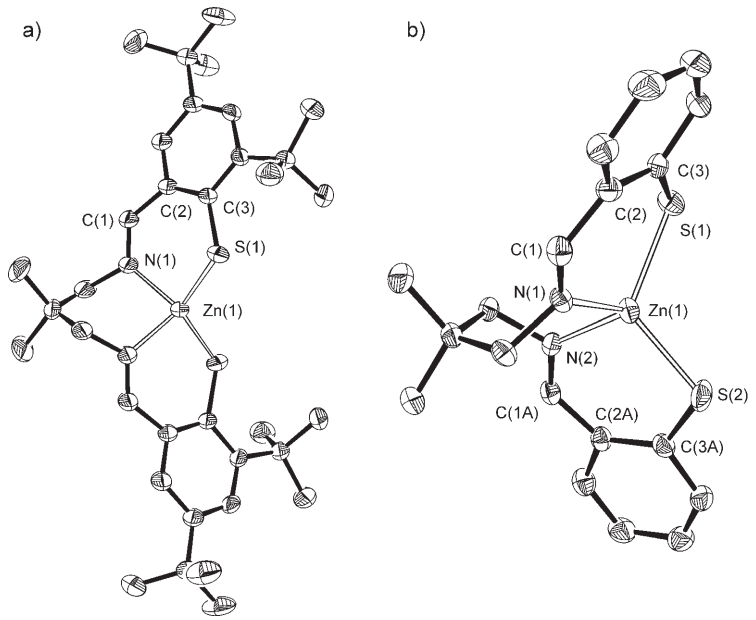

Figure 2. View of the molecular structure of a) **7** and b) **9** with displacement ellipsoids drawn at the 50% probability level. The H atoms are omitted for clarity.

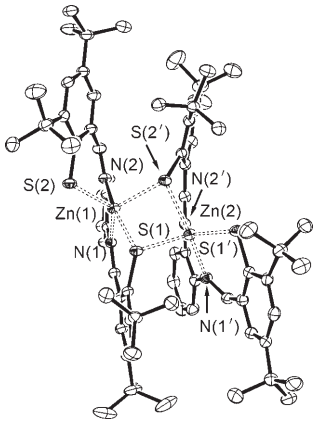

Figure 3. View of the molecular structure of $(\mathbf{8})_2$ with displacement ellipsoids drawn at the 50% probability level. The H atoms and molecules of MeCN are omitted for clarity.

when compared to previously reported syntheses of Ni-(tsalen)-type complexes as no thiol protection and deprotection steps are required.[33–36] Complexes **1**–**4** were obtained as analytically pure brown crystals by recrystallization from CH_2Cl_2. ^{1}H NMR and ^{13}C NMR measurements established the formation of diamagnetic Ni^{II} centers with significant upfield shifts in the peak positions compared to those observed for **7**–**10**.

X-ray crystal structures of 1–4: The Ni^{II} centers in **1**–**4** (Figure 4, see also Supporting Information SI1 and SI2) are bound by two thiolato S-donors and two imine N donors with the Ni(1)–S(1) and Ni(1)–S(2) bond lengths (ca. 2.16 Å, Table 4) lying within the range observed for previously reported Ni^{II}–S(thiolate) complexes.[17,18,37,38] The Ni(1)–N(1) and Ni(1)–N(2) distances (ca. 1.89 Å, Table 2) are typical of those observed for Ni^{II}–N(imine) bonds.[19,36,38–46] The dihedral angles between the planes defined by S(1)-Ni(1)-S(2) and N(1)-Ni(1)-N(2) (15.1, 21.1, 9.0 and 15.9° for **1**, **2**, **3** and **4**, respectively) indicate a distorted square-planar co-ordination environment about each Ni^{II} center. This distortion from planarity is greatest in **2** and **4** which results from the small N(1)-Ni(1)-N(2) bite angle (87.28(7) and 86.30(5)°, respectively, c.f. 91.16(7) and 90.12(9)° for **1** and **3**, respectively) enforced by the rigid 1,2-phenylenediimine backbone.

Electrochemistry: The cyclic voltammetry of **1** at 293 K in CH_2Cl_2 containing 0.4 M $[NnBu_4][BF_4]$ as supporting electrolyte reveals a reversible process at $E_{1/2}=0.16$ V versus Fc^+/Fc (Figure 5), and a second process at $E_p{}^a=0.82$ V versus Fc^+/Fc. Coulometric measurements confirm the process at $E_{1/2}=0.16$ V versus Fc^+/Fc as a one-electron oxidation, and variable-temperature cyclic voltammetric experiments over the range 291–226 K, reveal a temperature dependence (Figure 5). Similar observations have been made for the electrochemistry of $[Ni(ema)]^{2-}$ and $[Ni(pma)]^{2-}$ (H_4ema = *N*,*N*′-ethylenebis(2-mercaptoacetamide); H_4pma = *N*,*N*′-1,2-phenylenebis(2-mercaptoacetamide) which exhibit reversible oxidation processes at $E_{1/2}=-0.34$ and -0.24 V versus SCE in DMF, respectively, that become irreversible at −30 °C due to the likely formation of dimers involving the formation of a $Ni(\mu\text{-}SR)_2Ni$ bridge.[18]

The cyclic voltammogram of **2** shows (Figure 5) similar behavior and exhibits a reversible one-electron oxidation process at $E_{1/2}=0.10$ V versus Fc^+/Fc at 293 K that loses reversibility at temperatures below 253 K. In addition, a second, oxidation process is observed for **2** at $E_p{}^a=0.93$ V versus Fc^+/Fc at 293 K. By contrast, **3** and **4** do not exhibit any reversible redox processes; instead, a series of temperature-independent oxidative processes at $E_p{}^a=0.29$, 0.60 and 0.88 V versus Fc^+/Fc for **3** and $E_p{}^a=0.41$ V versus Fc^+/Fc for **4** were noted (see Figure S3 in the Supporting Information). This observation suggests that the incorporation of *t*Bu groups within the ligand frameworks in **1** and **2** stabilizes the one-electron oxidized species, $\mathbf{1}^+$ and $\mathbf{2}^+$ relative to the $\mathbf{3}^+$ and $\mathbf{4}^+$ under ambient conditions. This is consistent with the stability conferred by *t*Bu substitutions in Ni complexes containing salen-type phenolate ligands[47] and in $[Ni(^{bu}S_2)_2]^n$ ($n=2$, 1, 0; $^{bu}S_2$ = 3,5-ditertiarybutyl-1,2-benzenedithiolate).[48]

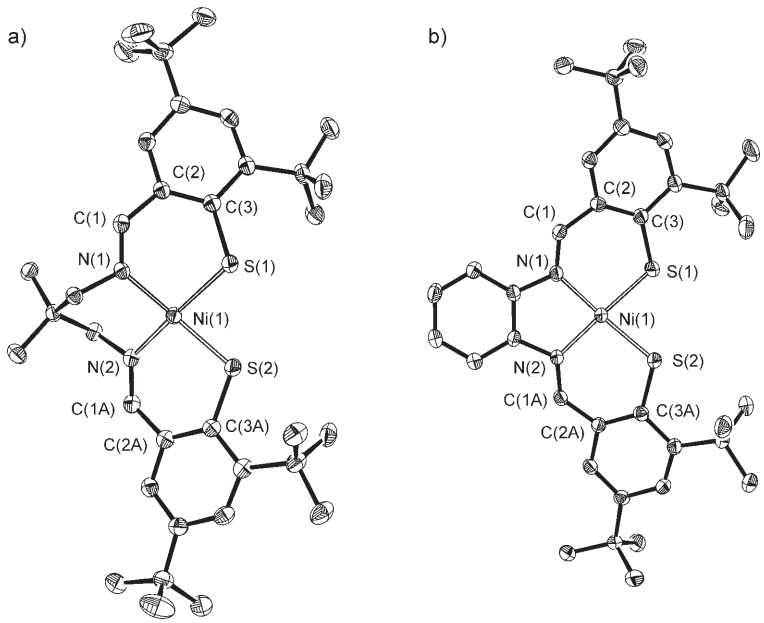

Figure 4. Views of the molecular structures of a) **1** and b) **2** with displacement ellipsoids drawn at the 50% probability level. H atoms are omitted for clarity.

Table 2. Selected bond lengths [Å] and angles [°] for **1**–**4** and $[(\mathbf{2})_2]^{2+}$.

	1	**2**	**3**	**4**	$[(\mathbf{2})_2]^{2+}$
Ni(1)−S(1)	2.1742(6)	2.1473(6)	2.1747(9)	2.1540(4)	2.138(4)
Ni(1)-S(2)	2.1577(6)	2.1407(6)	2.1681(9)	2.1614(4)	2.110(4)
Ni(1)−N(1)	1.902(2)	1.882(2)	1.917(2)	1.8993(13)	1.890(10)
Ni(1)−N(2)	1.898(2)	1.880(2)	1.924(2)	1.9061(12)	1.844(10)
Ni(2)−S(3)					2.153(3)
Ni(2)−S(4)					2.116(4)
Ni(2)−N(3)					1.888(10)
Ni(2)−N(4)					1.855(9)
S(1)−S(3)					2.202(5)
Ni(1)−Ni(2)					3.185(2)
S(1)−C(3)	1.763(2)	1.738(2)	1.748(3)	1.733(2)	
S(2)−C(3A)	1.761(2)	1.741(2)	1.744(3)	1.741(2)	
N(1)−C(1)	1.283(2)	1.316(2)	1.293(3)	1.302(2)	
N(2)−C(1A)	1.288(2)	1.318(2)	1.286(4)	1.298(2)	
S(1)-Ni(1)-S(2)	84.12(2)	83.33(2)	83.42(3)	81.91(2)	85.61(14)
S(1)-Ni(1)-N(1)	93.09(5)	96.08(5)	94.09(9)	97.10(4)	92.2(4)
S(1)-Ni(1)-N(2)	168.85(5)	165.39(5)	171.65(7)	169.01(4)	164.5(3)
S(2)-Ni(1)-N(1)	169.18(5)	165.79(5)	174.56(7)	169.24(4)	166.7(4)
S(2)-Ni(1)-N(2)	93.51(5)	96.86(5)	92.97(7)	96.67(4)	98.5(4)
N(1)-Ni(1)-N(2)	91.16(7)	87.28(7)	90.12(9)	86.30(5)	87.1(5)
S(3)-Ni(2)-S(4)					85.60(14)
S(3)-Ni(2)-N(3)					92.2(3)
S(3)-Ni(2)-N(4)					167.8(3)
S(4)-Ni(2)-N(3)					169.3(3)
S(4)-Ni(2)-N(4)					98.5(4)
N(3)-Ni(2)-N(4)					85.8(5)

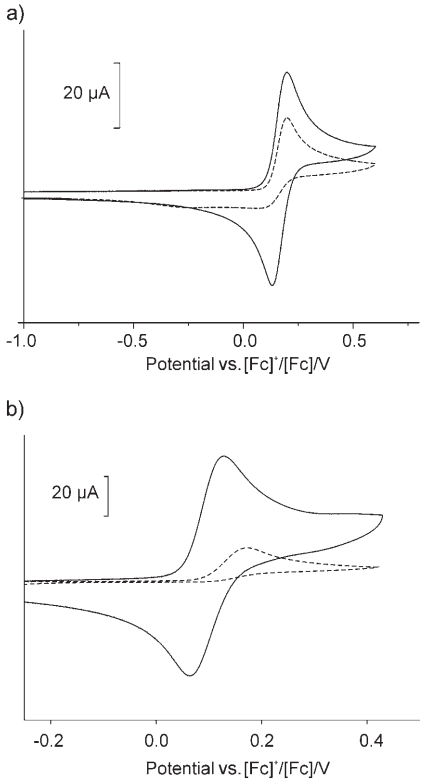

Figure 5. The cyclic voltammograms of a) **1** and b) **2** (1 mM), measured at 293 K (solid line) and 233 K (dashed line), in CH_2Cl_2 containing 0.4 M $[N\mathit{n}Bu_4][BF_4]$ as the supporting electrolyte at 100 mV s^{-1}.

EPR spectroscopy: Controlled potential electrolysis of **1** and **2** at 293 K in CH_2Cl_2 containing 0.4 M $[N\mathit{n}Bu_4][BF_4]$ as supporting electrolyte at applied potentials of 0.34 and 0.37 V versus Fc^+/Fc, respectively, affords green solutions of $\mathbf{1}^+$ and $\mathbf{2}^+$. Samples of $\mathbf{1}^+$ and $\mathbf{2}^+$ in CH_2Cl_2 were also prepared by chemical oxidation of **1** and **2**, respectively, with 70% $HClO_4$. At 293 K, the X-band EPR spectra of $\mathbf{1}^+$ and $\mathbf{2}^+$ exhibit isotropic signals at $g_{iso}=2.073$ and 2.064 with Gaussian linewidths of 16 G and 17 G, respectively, as determined by spectral simulations.[49] At 77 K, as frozen CH_2Cl_2 solutions, electrochemically generated $\mathbf{1}^+$ and $\mathbf{2}^+$, and $\mathbf{2}^+$ generated with $HClO_4$ are EPR-silent. In contrast, $\mathbf{1}^+$ generated by the reaction of **1** with $HClO_4$, is EPR-active at 77 K as a frozen CH_2Cl_2 solution, and exhibits a rhombic spectrum with $g_{11}=2.329$, $g_{22}=2.067$ and $g_{33}=2.027$ (Figure 6). The significant rhombic splitting of the g values and their unknown relationship to the molecular axis system does not permit an evaluation of the nature of the ground state in $\mathbf{1}^+$ solely on the basis of the experimental EPR spectroscopic data. Indeed the difficulties in deducing the ground states of low-spin d^7 complexes are well-documented.[18,50,51] However, it seems likely that binding of ClO_4^- to $\mathbf{1}^+$ is occurring under these conditions to afford **1**-ClO_4, the flexibility of the chelate ligand in $\mathbf{1}^+$ allowing coordination of the anion more readily compared to the more rigid, conjugated ligand in $\mathbf{2}^+$.

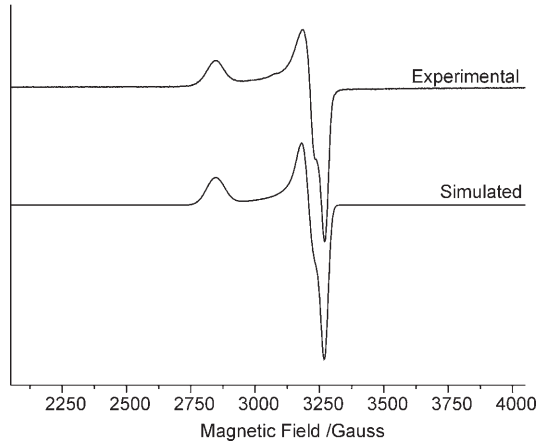

Figure 6. X-band EPR spectrum at 77 K of $HClO_4$ oxidized **1** in frozen CH_2Cl_2 solution. Spin Hamiltonian parameters $g_{11}=2.329$, $g_{22}=2.067$, and $g_{33}=2.027$ and Gaussian linewidths of $W_{11}=69$ G, $W_{22}=43$ G, and $W_{33}=28$ G.

Addition of pyridine to a frozen glass of **1**-ClO_4, followed by raising the temperature of the sample to about 193 K, and a subsequent refreezing of the sample enabled the 77 K frozen CH_2Cl_2 solution X-band EPR spectrum of [**1**$(py)_2$]ClO_4 to be recorded (Figure 7a). The observed anisotropy in the g tensors with $g_{11} \approx g_{22} \gg g_{33}$ is typical of a complex possessing an essentially Ni^{III} d_{z^2} ground-state.[18,52] Well-defined five-line hyperfine coupling to two ^{14}N ($I=1$) nuclei in the g_{33} region ($a_{33}=18.3$ G) is consistent with the co-ordination of two pyridine molecules to **1**$^+$ at axial sites about the Ni center. A similar treatment of **1**-ClO_4 with bipyridine yields [**1**(bipy)]ClO_4, the frozen solution X-band EPR spectrum of which reveals five-line hyperfine splitting in the g_{33} region ($a_{33}=18.5$ G) (Figure 7b) consistent with two ^{14}N nuclei bound to the Ni center. Fluid X-band EPR spectra of [**1**$(py)_2$]ClO_4 and [**1**(bipy)]ClO_4 could not be recorded because of the instability of these species above 195 K.

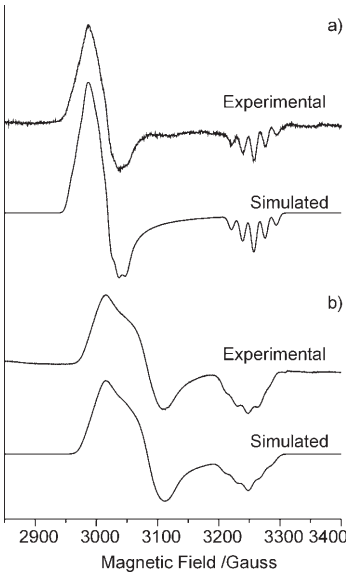

Figure 7. X-band EPR spectrum at 77 K of a) [**1**$(py)_2$]ClO_4 and b) [**1**(bipy)]ClO_4 in frozen CH_2Cl_2 solution. Spin Hamiltonian parameters for a) $g_{11}=2.218$, $g_{22}=2.192$, and $g_{33}=2.032$, $a_{11}=a_{22}=12$ G, $a_{33}=18.3$ G, Gaussian linewidths of $W_{11}=12$ G, $W_{22}=11$ G, and $W_{33}=9$ G for b) $g_{11}=2.198$, $g_{22}=2.147$, and $g_{33}=2.039$, $a_{11}=a_{22}=14$ G, $a_{33}=18.5$ G, Gaussian linewidths of $W_{11}=18$ G, $W_{22}=20$ G, and $W_{33}=16$ G.

UV/Vis spectroscopy: The UV/Vis spectrum of **1** exhibits well-defined absorptions at 406 ($\varepsilon_{max}=6200\,M^{-1}\,cm^{-1}$), 306 ($\varepsilon_{max}=25000\,M^{-1}\,cm^{-1}$), and 280 nm ($\varepsilon_{max}=38700\,M^{-1}\,cm^{-1}$). Shoulders are discernable at 477 ($\varepsilon_{max}=1700\,M^{-1}\,cm^{-1}$) and 587 nm ($\varepsilon_{max}=160\,M^{-1}\,cm^{-1}$). These lower energy features occur at wavelengths that are about 25 nm greater than those found in reduced NiSOD, at 450 and 563 nm, and which have been assigned to ligand-field transitions.[14] These transitions also compare with features at 461 ($\varepsilon_{max}=290\,M^{-1}\,cm^{-1}$) and 556 nm ($\varepsilon_{max}=70\,M^{-1}\,cm^{-1}$), respectively, observed for [Me_4N][Ni(BEAAM)].[20] The addition of pyridine to solutions of **1** at 293 and 253 K does not change the profile of the UV/Vis spectrum of **1**, suggesting that pyridine does not bind to **1** over this temperature range. The oxidation of **1** and **2** to **1**$^+$ and **2**$^+$, respectively, was monitored spectroelectrochemically using an optically transparent electrode cell (Figure 8). In the oxidation of **1** a new asymmetrically-shaped absorption appears at $\lambda_{max}=794$ nm ($\varepsilon_{max}=2900\,M^{-1}\,cm^{-1}$) together with a new shoulder at $\lambda_{max}=385$ nm ($\varepsilon_{max}=6700\,M^{-1}\,cm^{-1}$). Similar profiles have been obtained for [Ni(emb)]$^-$ (H_4emb=*N*,*N*′-ethylenebis(*o*-mercaptobenzamide), which exhibits[17] an intense absorption feature at 714 nm (ε_{max} ca. $4000\,M^{-1}\,cm^{-1}$) that has been assigned to S/N(π)→Ni(d_{π}^{*}) charge transfer.[13] The reversibility of the oxidation processes is confirmed by the electrochemical reduction of **1**$^+$ and **2**$^+$, which re-generates quantitatively the original spectra of **1** and **2**, respectively. The spectral features exhibited by electrochemically gener-

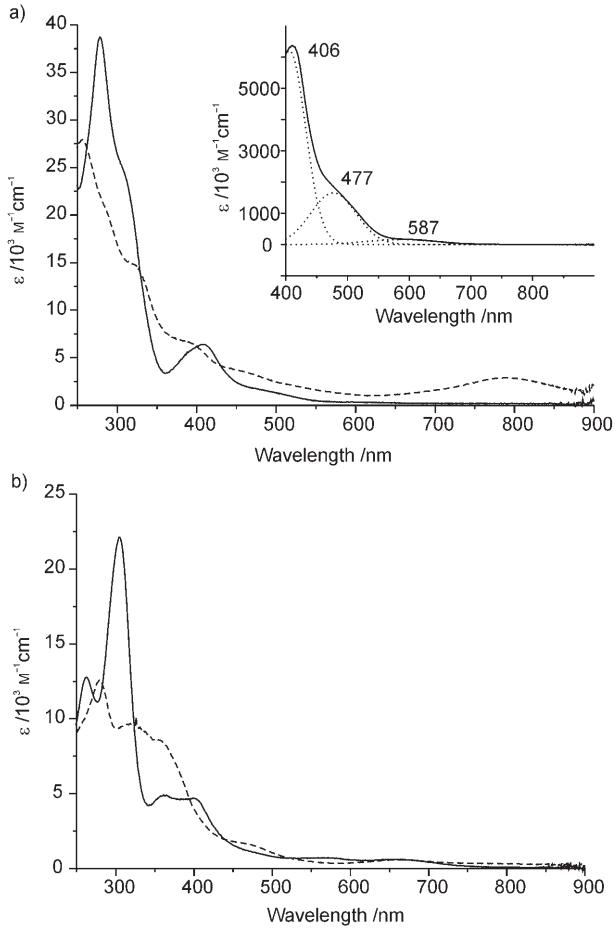

Figure 8. a) Electronic spectra of **1** (solid line) and electrochemically generated **1**$^+$ (broken line), 3.2×10^{-4} mol dm^{-3} at 293 K in CH_2Cl_2 containing 0.4 M [N*n*Bu$_4$][BF_4] as the supporting electrolyte. Inset: The Gaussian-deconvolved low-energy region of the electronic spectrum of **1**. b) Electronic spectra of **2** (solid line) and electrochemically-generated **2**$^+$ (broken line) at 293 K in CH_2Cl_2 containing 0.4 M [N*n*Bu$_4$][BF_4] as the supporting electrolyte

ated $\mathbf{1}^+$ are also observed upon chemical oxidation of **1** with one equivalent of $HClO_4$ in CH_2Cl_2 at 293 K.

The changes to the electronic spectra of electrochemically and chemically generated $\mathbf{1}^+$ in CH_2Cl_2 were monitored upon cooling from 293 K to 253 K. The features at $\lambda_{max}=385$ and 794 nm observed in UV/Vis spectra of $\mathbf{1}^+$ at 293 K are absent from the spectrum measured at 253 K (Figure 9a).

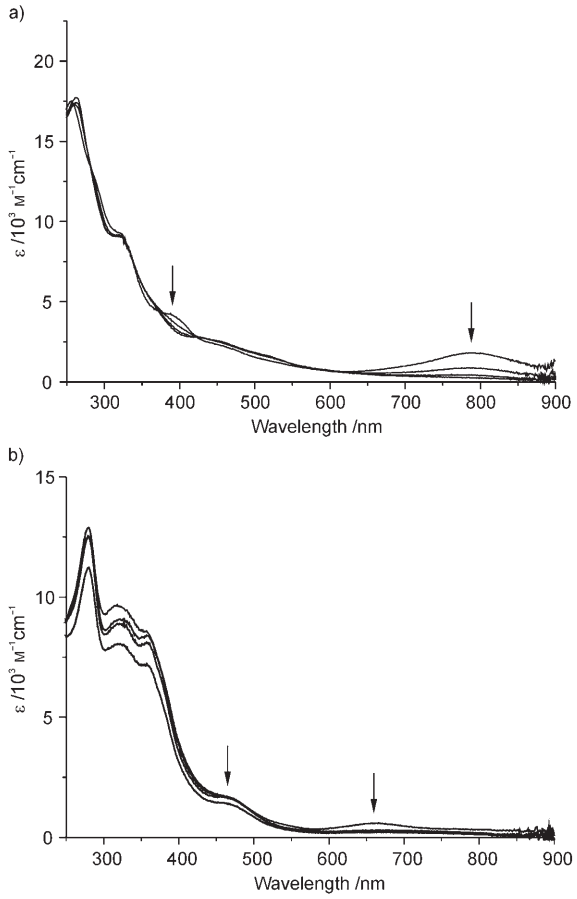

Figure 9. Changes in the electronic spectra of a) $\mathbf{1}^+$ on going from 293, 273, and 263, to 253 K and of b) $\mathbf{2}^+$ on going from 293, 272, and 253, to 233 K (3.2×10^{-4} mol dm^{-3} in CH_2Cl_2 containing 0.4 M $[N\mathit{n}Bu_4][BF_4]$ as the supporting electrolyte).

Subsequent warming of the sample to 293 K is accompanied by reappearance of these features and regeneration of the original spectrum of $\mathbf{1}^+$ at 293 K. The one-electron oxidation of **2** to $\mathbf{2}^+$ produces new features at $\lambda_{max}=665$ nm ($\varepsilon_{max}=590$ M^{-1} cm^{-1}) and $\lambda_{max}=460$ nm ($\varepsilon_{max}=1700$ M^{-1} cm^{-1}) that are similar to those of $\mathbf{1}^+$ (Figure 9). Electronic spectra recorded between 293 K and 253 K of solutions of $\mathbf{2}^+$ in CH_2Cl_2 show a disappearance of the band at 665 nm and its subsequent reappearance on the warming of the solution to 293 K (Figure 9b). This behavior is similar to that observed for $\mathbf{1}^+$. In addition, the UV/Vis spectra of electrochemically and chemically generated $\mathbf{1}^+$ and $\mathbf{2}^+$ below 293 K display significant deviations from the Beer–Lambert law between concentrations of 1.6×10^{-4} mol dm^{-3} and 3.2×10^{-3} mol dm^{-3}. Thus, $\mathbf{1}^+$ and $\mathbf{2}^+$ undergo a temperature- and concentration-dependent reversible chemical reaction or structural rearrangement at temperatures below 293 K that is consistent with the variable-temperature cyclic voltammetric studies detailed above.

X-ray crystal structure of $[(\mathbf{2})_2](ClO_4)_2\cdot2CH_2Cl_2$: Single crystals of $[(\mathbf{2})_2](ClO_4)_2\cdot2CH_2Cl_2$ suitable for X-ray crystallography were obtained by layering hexane onto a solution of $\mathbf{2}^+$ generated chemically by the oxidation of **2** with $HClO_4$ in CH_2Cl_2 followed by incubation at 195 K. The molecular structure of $[(\mathbf{2})_2](ClO_4)_2\cdot2CH_2Cl_2$ was determined crystallographically at 120 K, and selected bond lengths and angles are presented in Table 2. Views of the structure of the dication $[(\mathbf{2})_2]^{2+}$ are shown in Figure 10 and confirm that in the

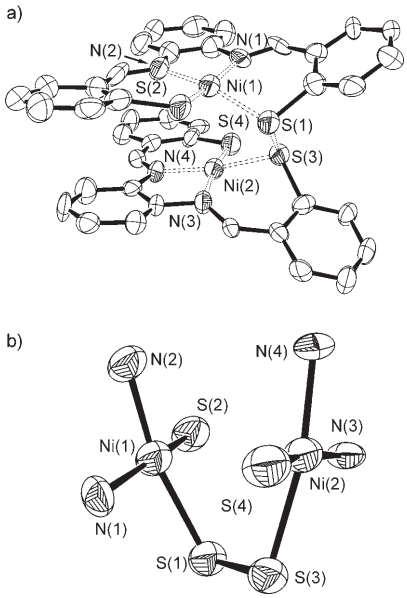

Figure 10. Views of the molecular structure of the dication in $[(\mathbf{2})_2](ClO_4)_2\cdot2CH_2Cl_2$ with displacement ellipsoids drawn at the 30% probability level. H atoms and *t*Bu groups are omitted for clarity.

solid-state two $\mathbf{2}^+$ units undergo a dimerization involving the formation of a single S–S bond (S(1)–S(3) 2.202(5) Å). The Ni(1)–Ni(2) distance (3.185(2) Å) is about 0.5 Å longer than the sum of the empirical radius of the Ni atom (1.35 Å),[53] which suggests that there is no formal Ni(1)–Ni(2) bond in $[(\mathbf{2})_2]^{2+}$. A tetragonal N_2S_2 coordination about each formal Ni^{II} center is maintained, and each Ni center possesses a distorted square-planar geometry with dihedral angles between the S-Ni-S and N-Ni-N planes of 20.6 and 16.2° for the planes incorporating Ni(1) and Ni(2), respectively. The S(1)–S(3) distance of 2.202(5) Å is about 0.15 Å longer than the typical distances observed in Ar-S-S-Ar disulfides.[38,39] The Ni(1)–S(1) and Ni(2)–S(3) distances (2.138(4) and 2.153(3) Å, respectively) are slightly longer than the Ni(1)–S(2) and Ni(2)–S(4) distances (2.112(4) and 2.116(4) Å, respectively) and are similar to the Ni(1)–S(1) and Ni(1)–S(2) bond lengths (2.1473(6) and 2.1407(6) Å, re-

spectively) in the parent complex **2**. The Ni–N distances vary from 1.890(10) to 1.842(10) Å in $[(\mathbf{2})_2]^{2+}$ and are similar to the Ni–N distances in **2** (Ni(1)–N(1) 1.882(2); Ni(1)–N(2) 1.880(2) Å) These observations confirm that Ni–SR cleavage does not occur on the formation of $[(\mathbf{2})_2]^{2+}$ in contrast to the oxidized complexes of Fe, Ga, and Co complexes with 1,4,7-triazacyclononane-1,4-diacetate containing a 2-mercaptobenzyl pendant arm.[54] In addition to the formation of a S–S bond, the stability of the dicationic dimer $[(\mathbf{2})_2]^{2+}$ is presumably augmented by intramolecular π–π stacking of the aromatic rings of the ligand frameworks.

The formation of $[(\mathbf{2})_2]^{2+}$ is in accord with the electrochemical, UV/Vis and EPR spectroscopic data for these systems, which confirm the formation of the paramagnetic Ni^{II}–thiyl radical species $\mathbf{1}^+$ and $\mathbf{2}^+$. These cations are in equilibrium in the absence of coordinating ligands/solvent with EPR-silent S–S bonded dimers $[(\mathbf{1})_2]^{2+}$ and $[(\mathbf{2})_2]^{2+}$, respectively. These dimeric species incorporate direct S–S bonding and since they are highly thermally and chemically sensitive, it was not possible to investigate these materials further.

DFT calculations: DFT calculations of models of **1** and **2** reproduce the principal features of the experimental geometries of **1–4**. The average calculated Ni–S and Ni–N distances for **1** (2.181 and 1.912 Å, respectively) compare well to the experimental distances of **3** (2.171 and 1.903 Å, respectively) and are similar to the experimental distances of **1** (2.166 and 1.900 Å, respectively). Similarly, the calculated Ni–S and Ni–N distances for **2** (2.164 and 1.908 Å, respectively) are comparable to the experimental distances of **4** (2.158 and 1.903 Å, respectively) and are similar to the experimental distances of **1** (2.144 and 1.851 Å, respectively). Moreover, the DFT calculations appear to support the significantly shorter Ni–S distances found in the X-ray crystallographic structures of complexes **2** and **4** relative to those of **1** and **3**. Thus, the close correspondence in metrical parameters for the experimental structures of **1–4** and the DFT-calculated structures for models of **1** and **2** suggests that the electronic structures of these centers, and their corresponding oxidized forms, are well described at the qualitative level by this DFT method.

Analyses of the electronic structures of **1** and **2** show that the redox-active orbital for these compounds is of π-symmetry and is composed of Ni $3d_{xz}$ (39%), Ni $3d_{x^2-y^2}$ (3%), S $3p_z$ (30%), S $3p_x$ (5%) and N $2p_z$ (1%) for **1** and Ni $3d_{xz}$ (42%), S $3p_z$ (31%), and N $2p_z$ (4%) for **2**, Figure 11a. The oxidation of models of **1** and **2** involves the removal of one electron from each of these orbitals to generate models of $\mathbf{1}^+$ and $\mathbf{2}^+$ possessing SOMOs with Ni $3d_{xz}$ (19%), Ni $3d_{x^2-y^2}$ (2%), S $3p_z$ (39%), S $3p_x$ (4%) and N $2p_z$ (2%) and, Ni $3d_{xz}$ (21%), S $3p_z$ (42%), and N $2p_z$ (3%) characters, respectively, Figure 11b. These orbitals are of the same symmetry as those of their parent orbitals in the models of **1** and **2** but with about 10% more S character. Thus, the oxidation of **1** and **2** appears to involve orbitals that possess considerable Ni–S covalency to produce a $[Ni(N_2S_2)]^+$ species with thiyl-radical character. The rhombic EPR spectrum for $\mathbf{1}^+$ (Figure 6) is consistent with a SOMO of π-symmetry, as revealed by the DFT calculations on models of $\mathbf{1}^+$ and $\mathbf{2}^+$. This symmetry is similar to that for the SOMO of $[Ni(emb)]^-$, which also exhibits a highly rhombic frozen solution EPR spectrum with $g_{11}=2.25$, $g_{22}=2.11$, and $g_{33}=2.04$.[13,17] The DFT calculations on the models of $\mathbf{1}^+$ and $\mathbf{2}^+$ also suggest that the SOMOs of these species are considerably more localized on the thiolate S donors than for the SOMO of $[Ni(emb)]^-$, which involves ca. 13% amide N character in addition to a 22% contribution from the S thiolate donors.[13] This greater contribution to the SOMO from the amide N-centers is consistent with the greater π-donor capacity of these donors in $[Ni(emb)]^-$ when compared to the imine N-donors in $\mathbf{1}^+$ and $\mathbf{2}^+$.

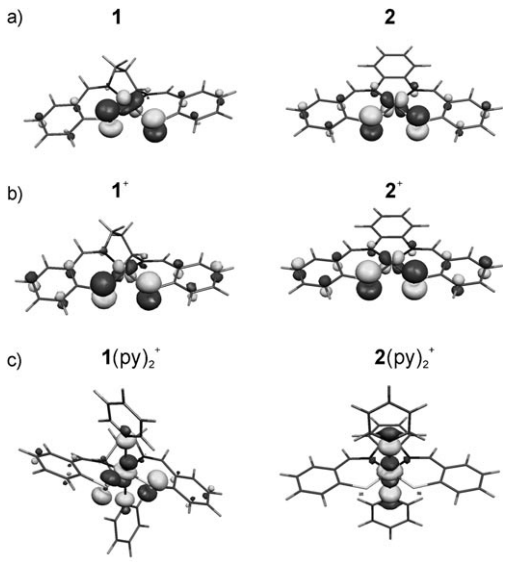

Figure 11. Kohn–Sham orbital isosurface plots at 0.05 eÅ^{-3} for a) the HOMOs of models of **1** and **2**, b) the SOMOs of models of $\mathbf{1}^+$ and $\mathbf{2}^+$, and c) the SOMOs of models of $\mathbf{1}(py)_2^+$ and $\mathbf{2}(py)_2^+$.

DFT calculations on models of $\mathbf{1}(py)_2^+$ and $\mathbf{2}(py)_2^+$ reveal SOMOs with substantially different compositions relative to those of their parent $\mathbf{1}^+$ and $\mathbf{2}^+$ models and which contain significant Ni $3d_{z^2}$ and N(py) character, Figure 11c. Thus, the composition of the SOMO in the model of $\mathbf{1}(py)_2^+$ is Ni $3d_{z^2}$ (29%), S 3p (25%), N(py) $2p_z$ (11%). and in the model of $\mathbf{2}(py)_2^+$ the composition is Ni $3d_{z^2}$ (47%), S 3p (7%), N(py) $2p_z$ (23%). This switch in SOMO on the binding of two pyridine ligands in the axial positions of the models of $\mathbf{1}^+$ and $\mathbf{2}^+$ is also supported by the frozen solution EPR spectrum of $\mathbf{1}(py)_2^+$ that is typical of a Ni^{III} center possessing a d_{z^2} ground state with ^{14}N hyperfine coupling in the g_{33} component. This hyperfine coupling is a consequence of the 2s and 2p N(py) contributions to the SOMO in $\mathbf{1}(py)_2^+$.

Conclusion

We have synthesized and crystallographically characterized the diamagnetic complexes $[Ni^{II}(N_2S_2)]$ containing thiolate

S- and imine N-donors and shown that **1** and **2** are capable of supporting reversible oxidation chemistry at room temperature. The analogous complexes **3** and **4** show an instability in their oxidized states indicating that *o*- and *p*-*t*Bu substitution of the thiolate rings limits decomposition pathways for the oxidized products, as has been found previously for phenolato metal complexes capable of supporting phenoxyl radical centers.[54–58] The EPR and UV/Vis spectroscopic measurements and supporting DFT calculations are consistent with the oxidation of **1** and **2** involving a π-type orbital with about 21% Ni and about 42–43% S character in the oxidized forms. Thus, the oxidation of **1** and **2** is largely ligand-based such that $\mathbf{1}^+$ and $\mathbf{2}^+$ possess considerable thiyl radical character. While similar ligand-based oxidation has been observed for $[Ni(emb)]^{2-}$, which also possesses phenyl thiolate units,[13,17] the incorporation of the poorer imine π-donors in $\mathbf{1}^+$ and $\mathbf{2}^+$ leads to greater contributions to the SOMO from the thiolate S-atoms in these complexes. DFT calculations[13] on $[Ni(ema)]^-$, which contains alkyl thiolate donors and which might be considered to be more relevant to the active site of NiSOD, result in an electronic structure that is analogous to $\mathbf{1}^+$, $\mathbf{2}^+$ and $[Ni(emb)]^-$. However, spectroscopic and DFT studies suggest that, in MeCN/propionitrile/butyronitrile solution, $[Ni(ema)]^-$ possesses a Ni^{III} center with a d_{z^2} ground state, most likely associated with the axial coordination of nitrile ligands.[13] Thus, $\mathbf{1}^+$, $\mathbf{2}^+$, $[Ni(ema)]^-$, and $[Ni(emb)]^-$ appear to exhibit similar oxidative chemistry suggesting that the incorporation of phenyl thiolate rather than alkyl thiolate donors has little impact on the ligand-based or metal-based nature of the ground states in these species.

Electrochemical, EPR and UV/Vis spectroscopic studies of $\mathbf{1}^+$ and $\mathbf{2}^+$ show that these species undergo a chemical process at temperatures below 293 K, that can be reversed on warming to ambient temperature, and the isolation and X-ray crystallographic characterization of $[(\mathbf{2})_2](ClO_4)_2 \cdot 2CH_2Cl_2$ shows that this reaction involves the formation of the diamagnetic $[(\mathbf{2})_2]^{2+}$ dimer. Similar variations in the spectroscopic and electrochemical properties of $[Ni(emb)]^-$ have also been rationalized in terms of a low-temperature dimerization process that may involve the formation of $[Ni_2(\mu\text{-}SR)_2]$ cores.[13,18] Additional support for this formulation has derived from parallel resonance Raman, UV/Vis and TD-DFT calculations.[13] For $\mathbf{2}^+$, our structural data show that $[(\mathbf{2})_2]^{2+}$ involves a S–S bond rather than the direct bridging of two of the S atoms across the bimetallic unit. The differences between the dimerization chemistry of $[Ni(emb)]^-$ and $\mathbf{2}^+$ may result from the greater S-atom contributions to the SOMO in $\mathbf{2}^+$ relative to those of $[Ni(emb)]^-$. This higher degree of thiyl radical character is a consequence of the differences in the π-donor strength of the N-atom donors in these complexes and may lead to the preferential formation of a disulfide in $[(\mathbf{2})_2]^{2+}$ as is commonly observed for the oxidation of thiolate in solution.[59] The relative instability and thermal sensitivity of both $[(\mathbf{1})_2]^{2+}$ and of $[(\mathbf{2})_2]^{2+}$ precluded further study of these materials.

The addition of pyridine to frozen solutions of $\mathbf{1}^+$ followed by warming to about 193 K and re-freezing leads to the generation of $\mathbf{1}(py)_2^+$ that possesses a SOMO with substantially less S character relative to $\mathbf{1}^+$ (ca. 29% vs. 42%, respectively) and with a dominant $3d_{z^2}$ character for the Ni contribution. For the calculated structure of $\mathbf{2}^+$, the imposition of C_{2v} symmetry prohibits combinations from S orbitals of π-type symmetry contributing to the SOMO. For this species the SOMO is almost exclusively derived from the Ni $3d_{z^2}$ and orbital combinations from the N(py) donor atoms. This switch in SOMO composition is reflected in the $g_{11} > g_{22} \gg g_{33}$ pattern and in the resolution of ^{14}N hyperfine coupling in the g_{33} region within the EPR spectrum of $\mathbf{1}(py)_2^+$. Thus, the coordination of axial N-donor ligands switches the SOMO from one which is essentially ligand-based to one that is more metal-based and which involves a formal Ni^{III} center. Our UV/Vis spectroscopic results suggest that pyridine binds only to $\mathbf{1}^+$ and not **1**. Therefore, $\mathbf{1}(py)_2^+$ can only form once **1** is oxidized to $\mathbf{1}^+$ followed by the binding of two pyridine donors to $\mathbf{1}^+$. This observation is consistent with the X-ray crystallographic results for NiSOD in its reduced and oxidized states and with recent spectroscopic and theoretical studies on the enzyme.[9,10,14] These latter studies point to a $O_2^{\bullet-}$ reduction step in which the redox active MO involves Ni/S/N(π) combinations to generate an oxidized species that is unbound by protein ligands at the axial sites of the Ni center. This unit subsequently binds an axial imidazole ligand to ensure a Ni^{III} SOMO with Ni $3d_{z^2}$ (76%) character and reduced S (9%) contributions. By comparison, the SOMO of the six coordinate complex $\mathbf{1}(py)_2^+$ contains significantly more S character (36%) than the SOMO of the five-coordinate oxidized form of the enzyme. Thus, even with the additional axial ligand in $\mathbf{1}(py)_2^+$, there is considerable S character within the SOMO of $\mathbf{1}(py)_2^+$. The differences in the compositions of the SOMOs of the oxidized form of NiSOD, in which the axial imidazole ligand has yet to bind and for those of the models of $\mathbf{1}^+$ and $\mathbf{2}^+$ are even more significant. The SOMO in this form of the enzyme possesses 58% Ni(π), 24% S(π), and 10% N/O(π) character,[14] whereas for $\mathbf{1}^+$ the SOMO possesses Ni (21%), S (43%) and N (2%) character. Thus, the active site of NiSOD appears to have evolved to minimize the S π-contributions in both the imidazole bound and un-bound forms of the oxidized enzyme whilst maintaining S-coordination to lower the redox potential of the metal center in the enzyme. The active site minimizes these S π-contributions in the redox-active orbital of the oxidized form by i) employing an amide ligand that is an effective π-donor in the imidazole un-bound form of the enzyme and ii) employing an axial imidazole ligand to switch the SOMO to an orbital that is essentially metal-based. In addition, our calculations indicate that the coordination geometry of the metal center and conformation of the ligand backbones play a major role in determining the composition of the redox-active orbitals.[60] This is most apparent for the calculations of $\mathbf{1}(py)_2^+$ and $\mathbf{2}(py)_2^+$; the latter complex, for which C_{2v} symmetry was imposed, possesses a SOMO that has no S π-character. Thus, it

is likely that the conformation of the protein side chains is also important in fine-tuning the nature of the electronic structure of the active site of NiSOD.

Experimental Section

Unless stated otherwise, all reactions were carried out under pure argon using standard Schlenk techniques. Where required, solvents were distilled by standard methods before use. All chemicals were purchased from Aldrich, except 1-formylpiperidine (Lancaster) and *tert*-butylchloride (Acros), and were used as received. 2,4-di-*tert*-butylbromobenzene was synthesized following literature preparations.[61–63] Complexes **3** and **9** and compound **6b** were prepared as described previously.[23]

NMR spectra were obtained using a Bruker DPX 300 spectrometer, and X-band EPR spectra were recorded on a Bruker EMX spectrometer with microwave frequencies calibrated with a Bruker ER035 M NMR gaussmeter. EPR spectra were simulated using WINEPR SimFonia Version 1.25 (Bruker). Infrared spectra were recorded with a Nicolet Avatar 360 FTIR spectrometer, and mass spectra were obtained from the EPSRC National Mass Spectrometry Service Center at the University of Wales, Swansea, UK. Elemental analyses were carried out by the Microanalytical Service at the University of Nottingham with an Exeter Analytical Inc CE-440 Elemental analyzer, and electrochemical measurements were performed with an Autolab PGSTAT20 potentiostat. Cyclic voltammograms were recorded using a three-electrode system consisting of a platinum working electrode, a platinum secondary electrode and an Ag/AgCl reference electrode. Experiments were carried out at 293 K, unless stated otherwise, under Ar using 1 mM solutions of complex in CH_2Cl_2 containing $[NnBu_4][BF_4]$ (0.4 M) as supporting electrolyte. Potentials are referenced to the Fc^+/Fc couple which was used as an internal standard. Where necessary, the $[FeCp^*_2]^+$/$[FeCp^*_2]$ couple was used as the internal standard to avoid overlapping of redox couples, and the $[FeCp^*_2]^+$/$[FeCp^*_2]$ couple was referenced to the Fc^+/Fc couple by an independent calibration. Compensation for internal resistance was not applied. Coulombic measurements were performed at 273 K under Ar in CH_2Cl_2 containing $[NnBu_4][BF_4]$ (0.4 M) as supporting electrolyte. A three-electrode system was used consisting of a Pt/Rh gauze basket working electrode, a Pt/Rh gauze secondary electrode and an Ag/AgCl reference electrode.

UV/Vis spectroelectrochemical measurements were carried out at 273 K using an optically transparent electrode mounted in a modified quartz cuvette with an optical pathlength of 0.5 mm. A three-electrode system was used consisting of a Pt/Rh gauze working electrode, a Pt wire secondary electrode in a fritted PTFE sleeve, and an Ag/AgCl reference electrode chemically isolated from the sample solution via a bridge tube containing electrolyte solution terminated in a porous frit. Potentials were applied using a Sycopel Scientific Ltd. DD10 M potentiostat and UV/Vis spectra recorded on a Perkin Elmer Lambda 16 Spectrometer. Temperature control was achieved by flowing cooled N_2 across the surface of the cell.

Synthesis of 2,4-di-*tert*-butylbenzenethiol (5a): A dry THF solution (40 mL) of 1-bromo-2,4-di-*tert*-butylbenzene (15.75 g, 58.5 mmol) was added dropwise to magnesium (4.46 g, 58.5 mmol) in THF (280 mL). The reaction mixture was heated at reflux for 45 min then cooled before addition of sulfur (1.88 g, 58.5 mmol) at 0 °C. The reaction mixture was stirred at 50 °C for 10 h. After the mixture was allowed to cool, the solution was decanted and carefully hydrolyzed with excess HCl (5%). THF was removed in vacuo and the crude product extracted with $CHCl_3$, washed with brine, and dried over $MgSO_4$. The $CHCl_3$ was then removed in vacuo and the product distilled (83 °C) by using a short-path Kugelruhr apparatus to give **5a** (12.15 g, 54.7 mmol, 94%). ^{1}H NMR (300 MHz, $CDCl_3$, 298 K, TMS): $\delta = 7.45$ (d, 1H, ArH), 7.19 (d, 1H, ArH), 7.07 (dd, 1H, ArH), 3.60 (s, 1H, SH), 1.52 (s, 9H, $C(CH_3)_3$), 1.35 ppm (s, 9H, $C(CH_3)_3$); MS (ES^+): *m/z*: 223 [**5a** + H^+].

Synthesis of 2,4-di-tert-butylthiosalicylaldehyde (6a): *n*BuLi (2.35 M, 9.13 mL, 21.5 mmol) was added to a solution of TMEDA (3.25 mL, 21.5 mmol) in anhydrous hexane (30 mL) at 0 °C followed by **5a** (2.2 g, 10 mmol). The reaction mixture was stirred at 0 °C for 30 min before being allowed to warm to room temperature and left to stir for 22 h. 1-Formylpiperidine (2.7 mL, 24 mmol) was added dropwise such that the temperature did not exceed 70 °C. The reaction mixture was stirred at room temperature for 16 h before the addition of aqueous HCl (5%, 100 mL). Et_2O (40 mL) was added and the organic layer separated. The aqueous layer was extracted with Et_2O (3×20 mL) and the organic extracts combined and dried over $MgSO_4$. Et_2O was removed in vacuo to give a viscous orange oil which was dissolved in hexane (5 mL) and passed through a short chromatographic column containing a silica/hexane slurry. A hexane/CH_2Cl_2 mixture with an increasing proportion of CH_2Cl_2 from 100:0 to 50:50 was passed through the column. The second fraction (ca. 75 mL) was collected, and the solvent removed in vacuo to give a viscous orange oil (**6a**, 1.48 g, 5.90 mmol, 59%), which was used without further purification.

Synthesis of 7·0.5H_2O: A solution of $Zn(OAc)_2{\cdot}2H_2O$ (0.58 g, 2.7 mmol) in MeOH (5 mL) was added to a solution of **6a** (1.20 g, 5.3 mmol) in MeCN (20 mL). A solution of triethylamine (0.81 g, 8.0 mmol) in MeOH (5 mL) was added to the mixture. A solution of 2-dimethyl-1,3-diaminopropane (0.22 g, 2.1 mmol) in MeOH (5 mL) was added dropwise to the orange solution. The reaction mixture was stirred for 1 h and then filtered to yield the crude product which was recrystallized from CH_2Cl_2 to give yellow crystals of **7** (1.51 g, 2.4 mmol, 90%). ^{1}H NMR (300 MHz, $CDCl_3$, 298 K, TMS): $\delta = 8.3$ (s, 2H, N=CH), 7.6 (d, 2H, ArH), 7.1 (d, 2H, ArH), 4.2 (bs, 2H, HC-H), 3.2 (bs, 2H, HC-H), 1.8 (s, 18H, $C(CH_3)_3$), 1.4 (s, 18H, $C(CH_3)_3$), 1.1 ppm (s, 6H, CH_3); ^{13}C NMR (75 MHz, $CDCl_3$, 298 K, TMS): δ = 171.6 (N=*C*H), 152.5 (Ar *C*H), 144.1(Ar *C*H), 143.9 (Ar *C*H), 131.9 (Ar *C*H), 131.7 (Ar *C*H), 128.1 (Ar *C*H), 68.4 (CH_2), 38.1 ($C(CH_3)_2$), 36.0 ($C(CH_3)_3$), 34.2 ($C(CH_3)_3$), 31.2 ($C(CH_3)_3$), 30.2 ($C(CH_3)_3$), 25.5 ppm ($C(CH_3)_2$); IR (KBr): $\tilde{\nu} = 2959$ s, 2907 m, 2867 m, 1637 s, 1599 w, 1466 m, 1386 m, 1361 m, 1263 m, 1200 w, 1155 m, 1080 w, 1049 m, 900 w, 744 w cm^{-1}; MS (ES^+): *m/z*: 630 [**7** + H^+]; elemental analysis calcd (%) for $C_{35}H_{52}N_2S_2Zn{\cdot}0.5H_2O$: C 65.75, H 8.36, N 4.38: found C: 65.95, H 8.12, N 4.45. Yellow crystals of **7** suitable for X-ray crystallography were obtained by slow diffusion of Et_2O onto a CH_2Cl_2 solution of **7**.

Synthesis of 8·0.5MeCN·H_2O: A solution of $Zn(OAc)_2{\cdot}2H_2O$ (0.58 g, 2.7 mmol) in MeOH (5 mL) was added to a solution of **6a** (1.20 g, 5.3 mmol) in MeCN (20 mL). A solution of triethylamine (0.81 g, 8.00 mmol) in MeOH (5 mL) was added to the mixture. The reaction flask was wrapped in foil and stirred in the dark during the dropwise addition of 1,2-phenylenediamine (0.23 g, 2.1 mmol) in MeOH (5 mL). The red mixture was stirred in the dark for 2 h by which time a precipitate had formed, the reaction was then stirred at 0 °C for a further 1 h after which time the reaction was exposed to light and the crude product separated by filtration. The precipitate was washed with cold MeOH and recrystallized from CH_2Cl_2 to give bright red crystals of **8** (1.41 g, 2.2 mmol, 84%). ^{1}H NMR (300 MHz, $CDCl_3$, 298 K, TMS): $\delta = 8.62$ (s, 2H, N=CH), 7.59 (d, 2H, ArH), 7.49 (m, 4H, ArH), 7.05 (d, 2H, ArH), 1.56 (s, 18H, $C(CH_3)_3$), 1.28 ppm (s, 18H, $C(CH_3)_3$); IR (KBr): $\tilde{\nu} = 2961$ vs, 2906 s, 2869 s, 1624 s, 1598 s, 1364 s, 1361 s, 1261 m, 1153 m, 1112 m, 1048 m, 1024 m cm^{-1}; MS (ES+): *m/z*: 637 [**8** + H^+]; elemental analysis calcd (%) for $C_{36}H_{46}N_2S_2Zn{\cdot}0.5CH_3CN{\cdot}H_2O$: C 65.86, H 7.39, N 5.19; found: C 66.13, H 7.07, N 4.83. Red crystals of (**8**)$_2$·MeCN suitable for X-ray crystallography were obtained by layering MeCN onto a CH_2Cl_2 solution of **8**.

Synthesis of 9·0.25H_2O: Compound **9**·0.25H_2O was prepared by literature methods from $Zn(OAc)_2{\cdot}2H_2O$, **6b**, and 2-dimethyl-1,3-diaminopropane.[23] ^{1}H NMR (300 MHz, $CDCl_3$, 298 K, TMS): δ = 8.30 (s, 2H, N=CH), 7.33 (d, 2H, ArH), 7.26 (d, 2H, ArH), 7.20 (t, 2H, ArH), 7.00 (t, 2H, ArH), 3.51 (bs, 4H, CH_2), 1.08 ppm (s, 6H, CH_3); ^{13}C NMR (75 MHz, $CDCl_3$, 298 K, TMS): $\delta = 170.6$ (N=CH), 137.1 (Ar CH), 137.1 (Ar CH), 131.1 (Ar CH), 129.4 (Ar CH), 122.4 (Ar CH), 122.4 (Ar CH), 68.3 (CH_2), 36.2 ($C(CH_3)_2$), 24.9 ppm ($C(CH_3)_2$); IR (KBr): $\tilde{\nu} = 2952$ w, 2917 w, 2863 w, 1632 s, 1587 m, 1540 m, 1462 m, 1442 w, 1409 m, 1391 w, 1336 w, 1252 w, 1203 w, 1162 w, 1127 m, 1065 m, 1027 m, 971 w, 868 w, 760 m, 752 m, 721 w, 686 w, 647 w cm^{-1}; MS (ES+): *m/z*: 405 [**9** + H^+]; elemental analysis calcd (%) for $C_{19}H_{20}N_2S_2Zn{\cdot}0.25H_2O$: C 55.62, H 5.04,

N 6.83: found: 55.92, H 4.94, N 6.65. Yellow crystals of **9** suitable for X-ray crystallography were obtained by slow evaporation of a solution of the complex in CH_2Cl_2.

Synthesis of 10·1.5H$_2$O: A solution of $Zn(OAc)_2{\cdot}2H_2O$ (0.55 g, 2.5 mmol) in MeOH (5 mL) was added to a solution of **6b** (5.00 mmol) in MeCN (20 mL). A solution of triethylamine (1.5 g, 15 mmol) in MeOH (5 mL) was added to the mixture. The reaction flask was wrapped in foil and stirred in the dark during the dropwise addition of 1,2-phenylenediamine (0.27 g, 2.5 mmol) in MeOH (5 mL). The red reaction mixture was stirred in the dark for 10 h during which time an insoluble precipitate formed. Filtration of the mixture gave **10** (0.95 g, 2.3 mmol, 92%) as a red powder, which was washed with cold MeOH and used without further purification. IR (KBr): $\tilde{\nu}$ = 2973 m, 1612 vs, 1602 vs, 1577 vs, 1526 s, 1451 s, 1399 s, 1183 s, 1126 m, 1075 m cm^{-1}; elemental analysis calcd (%) for $C_{20}H_{14}N_2S_2Zn{\cdot}1.5H_2O$: C 54.74, H 3.90, N 6.38; found: C 54.89, H 3.37, N 6.31.

Synthesis of 1·0.5H$_2$O: $Ni(NO_3)_2{\cdot}6H_2O$ (0.058 g, 0.19 mmol) in MeOH (3 mL) was added to a solution of **7**·0.5H$_2$O (0.126 g, 0.20 mmol) in CH_2Cl_2 (15 mL) and the solution stirred for 2 h. Excess MeOH was added to the brown solution and the precipitate collected by filtration in air. The crude product was washed with cold MeOH and recrystallized from CH_2Cl_2 to give brown crystals of **1** (0.11 g, 0.2 mmol, 92%). ^{1}H NMR (300 MHz, $CDCl_3$, 298 K, TMS): δ = 7.65 (s, 2H, N=CH), 7.42 (d, 2H, ArH), 7.07 (d, 2H, ArH), 3.55 (s, 4H, CH_2), 1.63 (s, 18H, C-(CH_3)$_3$), 1.28 (s, 18H, C(CH_3)$_3$), 1.03 ppm (s, 6H, CH_3); ^{13}C NMR (75 MHz, $CDCl_3$, 298 K, TMS): δ = 166.6 (N=CH), 149.5 (Ar *C*H), 133.0 (Ar *C*H), 128.3 (Ar *C*H), 127.5 (2 Ar *C*H), 127.5 (Ar *C*H), 69.5 (*C*H$_2$), 37.8 (*C*(CH$_3$)$_2$), 34.3 (*C*(CH$_3$)$_3$), 34.2 (*C*(CH$_3$)$_3$), 31.2 (C(*C*H$_3$)$_2$), 30.0 (C-(*C*H$_3$)$_2$), 24.8 ppm (C(*C*H$_3$)$_2$); IR (KBr): $\tilde{\nu}$ = 2959 vs, 2869 s, 1617 vs, 1463 s, 1388 s, 1361 s, 1266 s, 1230 m, 1163 m, 1059 m cm^{-1}; MS (ES+): *m/z*: 624 [**1** + H$^+$]; elemental analysis calcd (%) for $C_{35}H_{52}N_2S_2Ni.0.5H_2O$: C 66.45, H 8.44, N 4.43; found: C 66.55, H 8.35, N 4.38. Brown crystals of **1** suitable for X-ray crystallography were obtained by layering hexane onto a CH_2Cl_2 solution of the complex.

Synthesis of 2·MeOH: A solution of $Ni(NO_3)_2{\cdot}6H_2O$ (0.058 g, 0.19 mmol) in MeOH (3 mL) was added to a solution of **8**·0.5CH$_3$CN·H$_2$O (0.096 g, 0.14 mmol) in CH_2Cl_2 (20 mL). The dark brown solution was stirred for 1 h before concentration in vacuo to about 5 mL. Et$_2$O (2 mL) and hexane (30 mL) were added, and the brown solution cooled in ice for 1 h during which time a brown precipitate formed. The crude product was collected by filtration and washed with cold MeOH before being recrystallized from CH_2Cl_2 to give dark brown crystals of **2** (0.11 g, 0.18 mmol, 88%). ^{1}H NMR (300 MHz, $CDCl_3$, 298 K, TMS): δ = 9.00 (s, 2H, N=CH), 7.84 (q, 2H, ArH), 7.58 (d, 2H, ArH), 7.40 (q, 4H, ArH), 1.69 (s, 18H, C(CH$_3$)$_3$), 1.31 ppm (s, 18H, C-(CH$_3$)$_3$); ^{13}C NMR (75 MHz, $CDCl_3$, 298 K, TMS): δ = 159.2 (N=CH), 149.1 (Ar *C*H), 145.1 (Ar *C*H), 143.6 (Ar *C*H), 131.9 (Ar *C*H), 131.5 (Ar *C*H), 128.8 (Ar *C*H), 128.1 (Ar *C*H), 116.1 (Ar *C*H), 38.0 (*C*(CH$_3$)$_3$), 34.4 (*C*(CH$_3$)$_3$), 31.2 (C(*C*H$_3$)$_3$), 30.1 ppm (C(*C*H$_3$)$_3$); IR (KBr): $\tilde{\nu}$ = 2957 s, 2906 m, 2867 m, 1599 m, 1570 m, 1507 m, 1462 m, 1384 vs, 1362 m, 1161 m, 735 m cm^{-1}; MS (ES+): *m/z*: 629 [**2**$^+$]; elemental analysis calcd (%) for $C_{36}H_{46}N_2S_2Ni.CH_3OH$: C 67.17, H 7.62, N 4.23; found: C 67.39, H 7.20, N 3.81. Dark brown crystals of **2** suitable for X-ray crystallography were obtained by slow evaporation of MeOH from a 50:50 CH_2Cl_2/MeCN solution of the complex.

Synthesis of 3: Compound **3** was prepared from $Ni(NO_3)_2{\cdot}6H_2O$ and **9**·0.25H$_2$O by our method reported previously.[23] ^{1}H NMR (300 MHz, $CDCl_3$, 298 K, TMS): δ = 7.70 (s, 2H, N=CH), 7.26 (m, 4H, ArH), 7.19 (dd, 2H, ArH), 7.00 (dd, 2H, ArH), 3.62 (s, 4H, CH_2), 1.04 ppm (s, 6H, CH_3); ^{13}C NMR (75 MHz, $CDCl_3$, 298 K, TMS): δ = 165.2 (N=CH), 145.4 (Ar *C*H), 133.6 (Ar *C*H), 130.8 (Ar *C*H), 130.7 (Ar *C*H), 130.4 (Ar *C*H), 122.2 (Ar *C*H), 69.7 (*C*H$_2$), 34.8 (*C*(CH$_3$)$_2$), 24.4 ppm (C(*C*H$_3$)$_2$); IR (KBr): $\tilde{\nu}$ = 2959 s, 2924 s, 1615 vs, 1586 vs, 1540 s, 1446 s, 1427 m, 1389 m, 1221 s, 1128 m, 1079 s, 1061 m, 1035 m, 948 m, 747 vs, 720 m cm^{-1}; MS (ES+): *m/z*: 399 [**3** + H$^+$], 797 [(2×**3**) + H$^+$]; elemental analysis calcd (%) for $C_{19}H_{20}N_2S_2Ni$: C 57.17, H 5.05, N 7.02; found: C 57.19, H 5.08, N 6.94. Brown crystals of **3** suitable for X-ray crystallography were obtained by slow diffusion of Et$_2$O onto a CH_2Cl_2 solution of the complex.

Synthesis of 4·H$_2$O: A solution of $Ni(NO_3)_2{\cdot}6H_2O$ (0.058 g, 0.2 mmol) in MeOH (5 mL) was added with stirring to a suspension of **10**·1.5H$_2$O (0.082 g, 0.19 mmol) in CH_2Cl_2 (25 mL). The mixture was heated at 40 °C for 2 h during which time a slow transition from a red suspension to a dark brown solution occurred. The solution was concentrated in vacuo to about 7 mL and cold MeOH (40 mL) was added. The precipitate was collected by filtration and washed with cold MeOH followed by Et$_2$O before recrystallization from CH_2Cl_2 to give dark brown crystals of **4** (0.071 g, 0.17 mmol, 87%). ^{1}H NMR (300 MHz, $CDCl_3$, 298 K, TMS): δ = 8.95 (s, 2H, N=CH), 7.83 (m, 4H, ArH), 7.58 (dd, 2H, ArH), 7.41 (q, 2H, ArH), 7.28 (dd, 2H, ArH) , 7.08 ppm (td, 2H, ArH); ^{13}C NMR (75 MHz, $CDCl_3$, 298 K, TMS): δ = 157.9 (N=CH), 136.8 (Ar *C*H), 131.7 (Ar *C*H), 131.0 (Ar *C*H), 129.4 (Ar *C*H), 129.0 (Ar *C*H), 126.0 (Ar *C*H), 123.1 (Ar *C*H), 122.4 (Ar *C*H), 116.7 ppm (Ar *C*H); IR (KBr): $\tilde{\nu}$ = 1590 m, 1576 s, 1525 vs, 1457 vs, 1426 m, 1392 m, 1234 m, 1080 m, 748 s cm^{-1}; MS (ES+): *m/z* 406 [**4** + H$^+$], 810 [(2×**4**)$^+$]; elemental analysis calcd (%) for $C_{20}H_{14}N_2S_2Ni{\cdot}H_2O$: C 56.76, H 3.81, N 6.62; found: C 56.91, H 3.32, N 6.59. Dark brown crystals of **4** suitable for X-ray crystallography were obtained by slow evaporation of MeOH from a 50:50 CH_2Cl_2/MeOH solution of the complex.

X-ray crystallography: Crystallographic data and structure refinement parameters for complexes **1**–**4**, **7**, (**8**)$_2$·MeCN, **9** and (**2**)$_2$·(ClO$_4$)$_2$·2CH$_2$Cl$_2$ are summarized in Table 3 and Table 4. Crystals were mounted on a dual-stage glass fiber and diffraction measurements collected at 150(2) K on a Bruker SMART1000 (for **3**, **4**, **7**, **9**) or a Bruker SMART APEX CCD area diffractometer (for **1**, **2**, and (**8**)$_2$·MeCN) using graphite-monochromated Mo$_{K\alpha}$ radiation (λ = 0.71073 Å) and ω scans. Both diffractometers were equipped with an Oxford Cryosystems open-flow cryostat.[64] In the case of (**2**)$_2$·(ClO$_4$)$_2$·2CH$_2$Cl$_2$, diffraction measurements were collected at 120(2) K on a Bruker SMART APEX2 CCD area diffractometer using silicon [111]-monochromated synchrotron radiation (λ =

Table 3. Crystallographic data for **7**·0.13MeOH, (**8**)$_2$·MeCN, and **9**.

	7·0.13MeOH	(**8**)$_2$·MeCN	**9**
empirical formula	$C_{35.13}H_{52.5}N_2O_{0.13}S_2Zn$	$C_{74}H_{95}N_5S_4Zn_2$	$C_{19}H_{20}N_2S_2Zn$
M_r	634.28	1313.53	405.86
crystal system	monoclinic	triclinic	monoclinic
space group	*C*2/*c*	$P\bar{1}$	$P2_1$
a [Å]	32.560(2)	12.5404(8)	9.4649(11)
b [Å]	11.0318(9)	17.7470(11)	9.7759(11)
c [Å]	10.3704(7)	18.1994(12)	9.8843(11)
α [°]	90	67.259(2)	90
β [°]	104.921(2)	89.896(2)	95.914(2)
γ [°]	90	72.798(2)	90
volume [Å^3]	3599.4(7)	3539.2(4)	909.7(2)
Z	4	2	2
ρ_{calcd} [g cm^{-3}]	1.170	1.233	1.482
μ [mm^{-1}]	0.823	0.84	1.582
crystal size [mm]	0.31×0.18×0.16	0.51×0.40×0.12	0.25×0.22×0.10
reflections collected	11279	31481	5366
unique reflections (R_{int})	4419 (0.020)	15994 (0.020)	3334 (0.039)
R [F > 4σ(F)]	0.044	0.035	0.031
R_{wF} (all F^2)	0.134	0.095	0.068
GOF	1.046	1.03	0.995

Table 4. Crystallographic data for **1**–**4** and $[(\mathbf{2})_2](ClO_4)_2\cdot 2\,CH_2Cl_2$.

	1	**2**	**3**	**4**	$[(\mathbf{2})_2](ClO_4)_2\cdot 2\,CH_2Cl_2$
empirical formula	$C_{35}H_{52}N_2NiS_2$	$C_{36}H_{46}N_2NiS_2$	$C_{19}H_{20}N_2NiS_2$	$C_{20}H_{14}N_2NiS_2$	$C_{80}H_{110}Cl_6N_4Ni_2O_8S_4$
M_r	623.62	629.58	399.2	405.16	1714.08
crystal system	monoclinic	monoclinic	triclinic	monoclinic	monoclinic
space group	$P2_1/c$	$P2_1/c$	$P\bar{1}$	$P2_1/c$	$P2_1/c$
a [Å]	12.763(2)	8.1604(7)	8.5697(18)	6.9449(5)	24.296(5)
b [Å]	14.940(2)	25.658(2)	9.0569(19)	17.7885(13)	18.854(5)
c [Å]	18.229(3)	16.4775(13)	11.767(3)	13.5370(10)	18.330(5)
α [°]	90	90	76.164(3)	90	90
β [°]	93.030(3)	100.590(1)	87.506(3)	100.582(2)	111.067(5)
γ [°]	90	90	89.673(3)	90	90
volume [Å^3]	3471.0(2)	3391.2(8)	886.0(6)	1643.9(4)	7835(3)
Z	4	4	2	4	4
ρ_{calcd} [g cm^{-3}]	1.193	1.233	1.496	1.637	1.453
μ [mm^{-1}]	0.704	0.721	1.333	1.438	0.851[a]
crystal size [mm]	$0.33\times0.19\times0.15$	$0.28\times0.14\times0.04$	$0.25\times0.23\times0.04$	$0.49\times0.44\times0.22$	$0.02\times0.02\times0.02$
reflections collected	21583	23990	7692	14974	37375
unique reflections (R_{int})	8188 (0.024)	8084 (0.040)	3955 (0.033)	3895 (0.017)	8188 (0.1895)
R [$F>4\sigma(F)$]	0.043	0.039	0.040	0.023	0.088
R_{wF} (all F^2)	0.102	0.088	0.096	0.061	0.224
GOF	1.11	0.96	1.036	1.05	0.953

[a] $\lambda = 0.6868$ Å.

0.6868 Å) and ω scans from Daresbury SRS Station 9.8.[65,66] Empirical absorption corrections were applied using SADABS.[67] Structures were solved by direct methods using SHELXS-97[68] and, in the case of $(\mathbf{2})_2\cdot(ClO_4)_2\cdot 2\,CH_2Cl_2$, SIR-92[69] and refined with SHELXL-97.[70] Hydrogen atoms were geometrically placed in calculated positions and constrained to ride on their parent atom with $U_{iso}(H) = xU_{eq}$(parent), where x = 1.2 or 1.5.

DFT calculations: Calculations were performed by using the Amsterdam Density Functional (ADF) suite version 2005.01.[71] The open-shell restricted scalar relativistic DFT calculations employed a Slater type orbital (STO) triple-ζ-plus one polarization function all-electron basis sets from the ZORA/TZP database of the ADF suite for all atoms. The local density approximation (LDA) with the correlation potential due to Vosko et al.[72] was used in all of the DFT calculations. Gradient corrections were performed using the functionals of Becke[73] and Perdew (BP).[74] Models of **1**, $\mathbf{1}^+$, and $\mathbf{1}(py)_2^+$ were optimized without any symmetry constraints, whereas those of **2**, $\mathbf{2}^+$, and $\mathbf{2}(py)_2^+$ were optimized in idealized C_{2v} symmetry. The z axis is perpendicular to the NiS_2N_2 plane and the y axis bisects the N(1)-Ni-N(2) angle in the starting geometries in the coordinate frames employed in the calculations. Within each model, the *t*Bu groups of each thiolate ring were substituted by an H atom to decrease the computational effort required for the calculations.

CCDC-278858, CCDC-654478, CCDC-654479, CCDC-654480, CCDC-654481, CCDC-654482, CCDC-654483, CCDC-654484, CCDC-654485 contain the supplementary crystallographic data for this paper. These data can be obtained free of charge from The Cambridge Crystallographic Data Centre via www.ccdc.cam.ac.uk/data_request/cif.

Acknowledgements

We thank the EPSRC for financial support and CONACyT and DGAPA-UNAM for support to A. M.-B. We also thank the EPSRC National Service for Mass Spectrometry at the University of Wales, Swansea for mass spectra and the EPSRC X-ray Crystallography Service at the University of Southampton and the STFC Daresbury Laboratory for data collection from single crystals of $[(\mathbf{2})_2](ClO_4)_2\cdot 2\,CH_2Cl_2$. M.S. gratefully acknowledges receipt of a Royal Society Wolfson Merit Award and of a Royal Society Leverhulme Trust Senior Research Fellowship.

[1] a) Y. Higuchi, T. Yagi, N. Yasuoka, *Structure* **1997**, *5*, 1671–1680; b) Y. Higuchi, H. Ogata, K. Miki, N. Yasuoka, T. Yagi, *Structure* **1999**, *7*, 549–556; c) D. J. E. Spencer, A. C. Marr, M. Schröder, *Coord. Chem. Rev.* **2001**, *219–221*, 1055–1074.
[2] A. Volbeda, M. H. Charon, C. Piras, E. C. Hatchikian, M. Frey, J. C. Fontecilla-Camps, *Nature* **1995**, *373*, 580–587.
[3] V. Svetlitchnyi, H. Dobbek, W. Meyer-Klaucke, T. Meins, B. Thiele, P. Romer, R. Huber, O. Meyer, *Proc. Natl. Acad. Sci. USA* **2004**, *101*, 446–451.
[4] C. Darnault, A. Volbeda, E. J. Kim, P. Legrand, X. Vernede, P. A. Lindahl, J. C. Fontecilla-Camps, *Nat. Struct. Biol.* **2003**, *10*, 271–279.
[5] T. I. Doukov, T. M. Iverson, J. Seravalli, S. W. Ragsdale, C. L. Drennan, *Science* **2002**, *298*, 567–572.
[6] C. L. Drennan, J. Y. Heo, M. D. Sintchak, E. Schreiter, P. W. Ludden, *Proc. Natl. Acad. Sci. USA* **2001**, *98*, 11973–11978.
[7] H. Dobbek, V. Svetlitchnyi, L. Gremer, R. Huber, O. Meyer, *Science* **2001**, *293*, 1281–1285.
[8] U. Ermler, W. Grabarse, S. Shima, M. Goubeaud, R. K. Thauer, *Science* **1997**, *278*, 1457–1462.
[9] D. P. Barondeau, C. J. Kassmann, C. K. Bruns, J. A. Tainer, E. D. Getzoff, *Biochemistry* **2004**, *43*, 8038–8047.
[10] J. Wuerges, J-W. Lee, Y. I. Yim, H-S. Yim, S-O. Kang, K. Djinovic Carugo, *Proc. Natl. Acad. Sci. USA* **2004**, *101*, 8569–8574.
[11] A. F. Miller, *Curr. Opin. Chem. Biol.* **2004**, *8*, 162–168.
[12] J. S. Valentine, D. L. Wertz, T. J. Lyons, L. Liou, J. J. Goto, E. B. Gralla, *Curr. Opin. Chem. Biol.* **1998**, *2*, 253–262.
[13] A. T. Fiedler, T. C. Brunold, *Inorg. Chem.* **2007**, *46*, 8511–8523.
[14] A. T. Fiedler, P. A. Bryngelson, M. J. Maroney, T. C. Brunold, *J. Am. Chem. Soc.* **2005**, *127*, 5449–5462.
[15] C. A. Grapperhaus, M. Y. Darensbourg, *Acc. Chem. Res.* **1998**, *31*, 451–459.
[16] G. J. Colpas, M. Kumar, R. O. Day, M. J. Maroney, *Inorg. Chem.* **1990**, *29*, 4779–4788.
[17] H. Krüger, R. H. Holm, *Inorg. Chem.* **1987**, *26*, 3645–3647.
[18] H. Krüger, G. Peng, R. H. Holm, *Inorg. Chem.* **1991**, *30*, 734–742.
[19] H. J. Krüger, R. H. Holm, *J. Am. Chem. Soc.* **1990**, *112*, 2955–2963.
[20] J. Shearer, N. Zhao, *Inorg. Chem.* **2006**, *45*, 9637–9639.
[21] a) A. J. Blake, R. O. Gould, T. I. Hyde, M. Schröder, *J. Chem. Soc. Chem. Commun.* **1987**, 431–433; b) A. J. Blake, R. O. Gould, T. I. Hyde, M. Schröder, *J. Chem. Soc. Chem. Commun.* **1987**, 1730–1732; c) G. Reid, A. J. Blake, T. I. Hyde, M. Schröder, *J. Chem. Soc. Chem. Commun.* **1988**, 1397–1399; d) A. J. Blake, A. J. Holder, T. I.

Hyde, M. Schröder, *J. Chem. Soc. Chem. Commun.* **1987**, 987–988; e) A. J. Blake, L. M. Gordon, A. J. Holder, T. I. Hyde, G. Reid, M. Schröder, *J. Chem. Soc. Chem. Commun.* **1988**, 1452–1454; f) A. J. Blake, A. J. Holder, T. I. Hyde, M. Schröder, *J. Chem. Soc. Chem. Commun.* **1989**, 1433–1434; g) A. J. Blake, A. J. Holder, T. I. Hyde, H-J. Küppers, M. Schröder, S. Stötzel, K. Wieghardt, *J. Chem. Soc. Chem. Commun.* **1989**, 1600–1602; h) A. J. Blake, G. Reid, M. Schröder, *J. Chem. Soc. Dalton Trans.* **1990**, 3363–3373.

[22] a) C. W. G. Ansell, J. Lewis, P. R. Raithby, J. N. Ramsden, M. Schröder, *J. Chem. Soc. Chem. Commun.* **1982**, 546–547; b) J. Lewis, M. Schröder, *J. Chem. Soc. Dalton Trans.* **1982**, 1085–1089; c) A. J. Blake, R. O. Gould, M. A. Halcrow, A. J. Holder, T. I. Hyde, M. Schröder, *J. Chem. Soc. Dalton Trans.* **1992**, 3427–3431; d) N. D. M. J. Branscombe, A. J. Atkins, A. Marin-Becerra, E. J. L. McInnes, F. E. Mabbs, J. McMaster, M. Schröder, *Chem. Commun.* **2003**, 1098–1099; e) Q. Wang, E. Barclay, A. J. Blake, E. S. Davies, D. J. Evans, A. C. Marr, E. J. L. McInnes, J. McMaster, C. Wilson, M. Schröder, *Chem. Eur. J.* **2004**, *10*, 3384–3396; f) M-C. Chalbot, A. M. Mills, A. Spek, G. J. Long, E. Bouwman, *Eur. J. Inorg. Chem.* **2003**, 453–457; g) A. J. Amoroso, S. S. M. Chung, D. J. E. Spencer, M. G. Glenny, J. P. Danks, A. J. Blake, P. A. Cooke, C. Wilson, M. Schröder, *Chem. Commun.* **2003**, 2020–2021; h) W. Zhu, A. C. Marr, Q. Wang, F. Neese, D. J. E. Spencer, A. J. Blake, P. A. Cooke, C. Wilson, M. Schröder, *Proc. Natl. Acad. Sci. USA* **2005**, *102*, 18280–18285; i) A. Perra, E. S. Davies, J. R. Hyde, W. Qiang, J. McMaster, M. Schröder, *Chem. Commun.* **2006**, 1103–1105.

[23] P. A. Stenson, A. Marin-Becerra, A. J. Blake, C. Wilson, J. McMaster, M. Schröder, *Chem. Commun.* **2006**, 317–319.

[24] E. Block, V. Eswarakrishnan, M. Gernon, G. Ofori-Okai, C. Saha, K. Tang, J. Zubieta, *J. Am. Chem. Soc.* **1989**, *111*, 658–665.

[25] G. D. Figuly, C. K. Loop, J. C. Martin, *J. Am. Chem. Soc.* **1989**, *111*, 654–658.

[26] D. M. Giolando, K. Kirschbaum, *Synthesis* **1992**, 451–452.

[27] U. Brand, H. Vahrenkamp, *Chem. Ber.* **1995**, *128*, 787–791.

[28] A. R. Cowley, J. R. Dilworth, P. S. Donnelly, E. Labisbal, A. Sousa, *J. Am. Chem. Soc.* **2002**, *124*, 5270–5271.

[29] V. L. Goedken, G. G. Christoph, *Inorg. Chem.* **1973**, *12*, 2316–2320.

[30] D. J. E. Spencer, A. J. Blake, S. Parsons, M. Schröder, *J. Chem. Soc. Dalton Trans.* **1999**, 1041–1042.

[31] V. V. Tkachev, E. A. Kordrashkina, L. O. Atovmyan, *J. Struct. Chem.* **1977**, *18*, 833–841.

[32] T. Tuntulani, J. H. Reibenspies, P. J. Farmer, M. Y. Darensbourg, *Inorg. Chem.* **1992**, *31*, 3497–3499.

[33] M. F. Corrigan, B. O. West, *Aust. J. Chem.* **1976**, *29*, 1413–1427.

[34] N. Goswami, D. M. Eichhorn, *Inorg. Chem.* **1999**, *38*, 4329–4333.

[35] N. Goswami, D. M. Eichhorn, *Inorg. Chim. Acta* **2000**, *303*, 271–276.

[36] T. Yamamura, M. Tadokoro, R. Kuroda, *Chem. Lett.* **1989**, 1245–1246.

[37] S. Fox, Y. Wang, A. Silver, M. J. Millar, *J. Am. Chem. Soc.* **1990**, *112*, 3218–3220.

[38] W. J. J. Smeets, A. Spek, R. K. Henderson, E. Bouwman, J. Reedijk, *Acta Crystallogr. Sect. C* **1997**, 53, 1564–1566.

[39] F. H. Allen, *J. Acta. Crystallogr. Sect. B.* **2002**, *58*, 380–388.

[40] A. J. Atkins, D. Black, A. J. Blake, A. Marin-Becerra, S. Parsons, L. Ruiz-Ramirez, M. Schröder, *Chem. Commun.* **1996**, 457–464.

[41] A. J. Atkins, A. J. Blake, M. Schröder, *J. Chem. Soc. Chem. Commun.* **1993**, 1662–1665.

[42] N. D. J. Branscombe, A. J. Blake, A. Marin-Becerra, W .S. Li, S. Parsons, L. Ruiz-Ramirez, M. Schröder, *Chem. Commun.* **1996**, 2573–2574.

[43] J. Hanss, H. J. Krüger, *Angew. Chem.* **1998**, *110*, 366–369; *Angew. Chem. Int. Ed.* **1998**, *37*, 360–363.

[44] D. Sellmann, F. Geipel, F. Lauderbach, F. W. Heinemann, *Angew. Chem.* **2002**, *114*, 654–656; *Angew. Chem. Int. Ed.* **2002**, *41*, 632–634; .

[45] D. Sellmann, R. Prakash, F. W. Heinemann, *Eur. J. Inorg. Chem.* **2004**, *10*, 1847–1858.

[46] G. Steinfeld, B. Kersting, *Chem. Commun.* **2000**, 205–206.

[47] O. Rotthaus, F. Thomas, O. Jarjayes, C. Philouze, E. Saint-Aman, J. L. Pierre, *Chem. Eur. J.* **2006**, *12*, 6953–6962.

[48] D. Sellmann, H. Binder, D. Häußinger, F. W. Heinemann, J. Sutter, *Inorg. Chim. Acta* **2000**, *300–302*, 829–836.

[49] F. E. Mabbs, D. Collinson, *Electron Paramagnetic Resonance of d-Transition Metal Compounds*, Elsevier, Amsterdam, **1992**.

[50] B. R. McGarvey, *Can. J. Chem.* **1975**, *53*, 2498–2511.

[51] Y. Nishida, S. Kida, *Bull. Chem. Soc. Jpn.* **1978**, *51*, 143–149.

[52] N. Takvoryan, K. Farmery, V. Katovic, F. V. Lovecchio, E. S. Gore, L. B. Anderson, D. H. Busch, *J. Am. Chem. Soc.* **1974**, *96*, 731–742.

[53] J. C. Slater, *J. Chem. Phys.* **1964**, *41*, 3199–3204.

[54] a) S. Kimura, E. Bill, E. Bothe, T. Weyhermüller, K. Wieghardt, *J. Am. Chem. Soc.* **2001**, *123*, 6025–6039; b) T. Glaser, T. Beissel, E. Bill, T. Weyhermüller, V. Schunemann, W. Meyer-Klauke, A. X. Trautwein, K. Wieghardt, *J. Am. Chem. Soc.* **1999**, *121*, 2193–2208; c) T. Glaser, T. Beissel, E. Bill, T. Weyhermüller, W. Meyer-Klauke, K. Wieghardt, *Inorg. Chem.* **1999**, *38*, 722–732; d) G. Steinfeld, B. Kersting, *Chem. Commun.* **2000**, *3*, 205–206.

[55] L. Benisvy, E. Bill, A. J. Blake, D. Collison, E. S. Davies, C. D. Garner, C. I. Guindy, E. J. L. McInnes, G. McArdle, J. McMaster, C. Wilson, J. Wolowska, *Dalton Trans.* **2004**, 3647–3653.

[56] L. Benisvy, E. Bill, A. J. Blake, D. Collison, E. S. Davies, C. D. Garner, G. McArdle, E. J. L. McInnes, J. McMaster, S. H. K. Ross, C. Wilson, *Dalton Trans.* **2006**, 258–267.

[57] L. Benisvy, A. J. Blake, D. Collison, E. S. Davies, C. D. Garner, E. J. L. McInnes, J. McMaster, G. Whittaker, C. Wilson, *Chem. Commun.* **2001**, 1824–1825.

[58] L. Benisvy, A. J. Blake, D. Collison, E. S. Davies, C. D. Garner, E. J. L. McInnes, J. McMaster, G. Whittaker, C. Wilson, *Dalton Trans.* **2003**, 1975–1985.

[59] J. K. Howie, J. J. Houts, D. T. Sawyer, *J. Am. Chem. Soc.* **1977**, *99*, 6323–6326.

[60] C. S. Mullins, C. A. Grapperhaus, P. M. Kozlowski, *J. Biol. Inorg. Chem.* **2006**, *11*, 617–625.

[61] R. Edler, J. Voss, *Chem. Ber.* **1989**, *122*, 187–191.

[62] C. M. D. Komen, F. Bickelhaupt, *Synth. Commun.* **1996**, *26*, 1693–1697.

[63] P. C. Myhre, T. Reiger, J. T. Stone, *J. Org. Chem.* **1966**, *31*, 3425–3426.

[64] J. Cosier, A. M. Glazer, *J. Appl. Crystallogr.* **1986**, *19*, 105–107.

[65] R. J. Cernik, W. Clegg, C. R. A. Catlow, G. Bushnell-Wye, J. V. Flaherty, G. N. Greaves, M. Hamichi, I. Burrows, D. J. Taylor, S. J. Teat, *J. Synchrotron Radiat.* **1997**, *4*, 279–286.

[66] W. Clegg, *J. Chem. Soc. Dalton Trans.* **2000**, 3223–3232.

[67] G. M. Sheldrick, SADABS, Program for Correcting Area Detector Data, Bruker AXS Inc., Madison, Wisconsin, USA, **2001**.

[68] G. M. Sheldrick, SHELXS-97, Program for Crystal Structure Solution, University of Göttingen, Göttingen, Germany, **1997**.

[69] A. Altomare, G. Cascaravo, C. Giacovazzo, A. Gualardi, *J. Appl. Crystallogr.* **1993**, *26*, 343–350.

[70] G. M. Sheldrick, SHELXL-97, Program for Crystal Structure Refinement, University of Göttingen, Göttingen, Germany, **1997**.

[71] SCM, Vrije Universiteit Amsterdam; http://www.scm.com, Amsterdam, The Netherlands; C. F. Guerra, J. G. Snijders, G. te Velde, E. J. Baerends, *Theor. Chem. Acc.* **1998**, *99*, 391–403; G. te Velde, F. M. Bickelhaupt, S. J. A. van Gisbergen, G. C. Fonseca, E. J. Baerends, J. G. Snijders, T. Ziegler, *J. Comput. Chem.* **2001**, *22*, 931–967.

[72] S. H. Vosko, L. Wilk, M. Nusair, *Can. J. Phys.* **1980**, *58*, 1200–1211.

[73] A. D. Becke, *Phys. Rev. A* **1988**, *38*, 3098–3100.

[74] J. P. Perdew, *Phys. Rev. B* **1986**, *33*, 8822–8824.

Received: July 18, 2007
Published online: January 21, 2008

